

Van Der Waals Heterostructures with Spin-Orbit Coupling

Enrico Rossi* and Christopher Triola

Herein, recent work on van der Waals (vdW) systems in which at least one of the components has strong spin-orbit coupling is reviewed, focussing on a selection of vdW heterostructures to exemplify the type of interesting electronic properties that can arise in these systems. First a general effective model to describe the low energy electronic degrees of freedom in these systems is presented. The model is then applied to study the case of (vdW) systems formed by a graphene sheet and a topological insulator. The electronic transport properties of such systems are discussed and it is shown how they exhibit much stronger spin-dependent transport effects than isolated topological insulators. Then, vdW systems are considered in which the layer with strong spin-orbit coupling is a monolayer transition metal dichalcogenide (TMD) and graphene-TMD systems are briefly discussed. In the second part of the article, a case is discussed in which the vdW system includes a superconducting layer in addition to the layer with strong spin-orbit coupling. It is shown in detail how these systems can be designed to realize odd-frequency superconducting pair correlations. Finally, twisted graphene-NbSe₂ bilayer systems are discussed as an example in which the strength of the proximity-induced superconducting pairing in the normal layer, and its Ising character, can be tuned via the relative twist angle between the two layers forming the heterostructure.

the fact that this is now experimentally feasible. Experimentalists are able to isolate layers of different materials only one-atom, or few-atoms, thick, and to combine such layers with increasing control of the stacking configuration. A striking example of this tunability is the recent experimental realization of vdW systems formed by two graphene layers in which the stacking angle, twist angle, can be adjusted to within a fraction of a degree.^[8–10] These experiments^[8–10] have shown that, by tuning the relative twist angle between graphene layers, the system can become superconducting or insulating. These remarkable results are just one example of the ways in which vdW heterostructures can be used to realize electronic systems with exotic and desirable properties.

Of particular interest are the recent developments involving vdW systems comprised of two layers in which one of the layers has a strong spin-orbit coupling (SOC). The main interest in these systems arises from the possibility of realizing novel electronic systems by

1. Introduction


Van der Waals (vdW) heterostructures^[1–4] represent a growing class of systems which are formed from 2D layers of material held to one another by only van der Waals forces. One of the most common vdW heterostructures, graphite, is composed entirely of layered sheets of graphene,^[5–7] a one-atom thick 2D crystal of carbon atoms arranged in a honeycomb structure. The nature of the vdW force implies that in a vdW system the stacking configuration of the layers is not dictated by chemistry but, to a great extent, can be tuned arbitrarily in an almost continuous way. The explosion of interest in vdW systems stems from

combining such a layer with a different layer which possesses little or no SOC but with other interesting properties. For example, graphene possesses only very weak SOC but has very high electron mobility at room temperature. By combining graphene with the 2D surface of a 3D topological insulator (TI),^[11–13] the SOC in the graphene layer can be enhanced by an order of magnitude.^[14,15] Additionally, as we discuss in Section 5.1, vdW heterostructures with SOC appear to be ideal systems for realizing unconventional odd-frequency superconducting states.^[16] In contrast to conventional superconducting states, the defining feature of odd-frequency superconductors is that they host Cooper pairs which are odd functions in the relative time, making these states intrinsically dynamical.

The literature on vdW systems is by now very large, for this reason we restrict ourselves to a particular subset of vdW systems that are among the most relevant to the subject of this special issue and that we have studied over the past few years. We first present, in Section 2, the model to describe vdW systems with SOC. To exemplify the application of this general formalism, in Section 3, we discuss the case of vdW heterostructures formed by graphene and a TI. In Section 4, we discuss recent progress on vdW systems which include both graphene and a layer of transition metal dichalcogenide (TMD). We then consider, in Section 5, the case in which one of the layers is a superconductor, discussing the possibility of realizing different exotic superconducting states

Dr. E. Rossi
Department of Physics
William & Mary
Williamsburg, VA 23188, USA
E-mail: erossi@wm.edu

Dr. C. Triola
Department of Physics and Astronomy
Uppsala University
Box 516, S-751 20 Uppsala, Sweden

 The ORCID identification number(s) for the author(s) of this article can be found under <https://doi.org/10.1002/andp.201900344>

DOI: 10.1002/andp.201900344

in vdW systems with SOC. In Section 6 we present our conclusion and outlook for future developments.

While the focus of this article is primarily on vdW systems composed of graphene, topological insulators, and TMDs, we note that much progress has also been made studying vdW systems with other components. Notably, we do not discuss the recently discovered 2D magnetic materials,^[17–19] which include: FePS₃,^[20] Cr₂GeTe₆,^[21] CrI₃,^[22,23] VSe₂,^[24] MnSe_x,^[25] and Fe₃GeTe₂.^[26,27] Similarly, we do not cover the magnetic proximity effect^[28] which has been discussed in a variety of vdW heterostructures.^[29–31] We also omit discussion of the intriguing heterostructures which can be made using monolayers with buckled honeycomb structure –silicene,^[32] germanene,^[33,34] and stanene^[35] –systems involving nanoribbons,^[36] and structures formed by different layers of TMDs^[37] and twisted TMD homobilayers.^[38–41]

2. Model

The Hamiltonian describing a generic double-layer vdW system can be written as $H = H_1 + H_2 + H_t$, where H_ℓ ($\ell = 1, 2$) is the Hamiltonian associated with layer ℓ and H_t describes tunneling processes between the two layers. Here, we write $H_1 = \sum_{k\alpha\alpha'} c_{k\alpha}^\dagger h(\mathbf{k})_{1;\alpha\alpha'} c_{k\alpha'}$, $H_2 = \sum_{k\alpha\alpha'} d_{k\alpha}^\dagger h(\mathbf{k})_{2;\alpha\alpha'} d_{k\alpha'}$, where $c_{k\alpha}^\dagger$ and $d_{k\alpha}^\dagger$ ($c_{k\alpha}$ and $d_{k\alpha}$) create (annihilate) single electron states in layers 1 and 2, respectively, with momentum \mathbf{k} and all other degrees of freedom described by the composite index α , including spin, orbital, and particle-hole degrees of freedom. We assume that the tunneling between the two layers depends only on the difference between the positions, \mathbf{r}_1 , \mathbf{r}_2 , of the electrons in the two layers. As a consequence, the crystal momentum is conserved during tunneling processes and we have

$$H_t = \sum_{\mathbf{k}_1 \mathbf{k}_2} \sum_{\mathbf{G}_1 \mathbf{G}_2} \sum_{\alpha_1 \alpha_2} \sum_{s_1 s_2} t_{\alpha_1 \alpha_2}(\mathbf{k}_1 + \mathbf{G}_1) e^{i\mathbf{G}_2 \cdot \boldsymbol{\tau}_{s_2} - i\mathbf{G}_1 \cdot \boldsymbol{\tau}_{s_1}} \times c_{\mathbf{k}_1 \alpha_1}^\dagger d_{\mathbf{k}_2 + (\mathbf{G}_2 - \mathbf{G}_1) \alpha_2} + \text{h.c.} \quad (1)$$

where \mathbf{G}_ℓ is the reciprocal lattice vector in layer ℓ and we have allowed for the possibility that the lattices making-up each of the two layers may possess basis vectors $\boldsymbol{\tau}_{s_\ell}$. For example, for the case of graphene we have two basis vectors $\boldsymbol{\tau}_s$, which we can write as $\boldsymbol{\tau}_s = \{(0, 0); (a_0, 0)\}$, where a_0 is the carbon–carbon distance.

In a bilayer vdW system, two very different kinds of stacking are possible: commensurate stacking, and incommensurate stacking. In the first case, the vdW bilayer has a periodic structure in real space with a large primitive cell that is commensurate with the primitive cells of both layers. In the incommensurate case, no such periodicity exists in real space. For the commensurate case we obtain a well defined Moiré pattern.

Given two layers ($\ell = 1, 2$) with primitive lattice vectors $\mathbf{a}_{\ell i}$ ($i = 1, 2$), in order for a stacking to be commensurate there must exist four integers m_1, m_2, n_1, n_2 such that:

$$m_1 \mathbf{a}_{11} + m_2 \mathbf{a}_{12} = n_1 \mathbf{a}_{21} + n_2 \mathbf{a}_{22} \quad (2)$$

Without loss of generality, using complex numbers to represent 2D vectors, we can write $\mathbf{a}_{11} = a_{10} e^{-i\theta_1}$, $\mathbf{a}_{12} = a_{10} e^{+i\theta_1}$, $\mathbf{a}_{21} =$



physics faculty at William & Mary in 2010.

Enrico Rossi received his Ph.D. from the University of Texas at Austin in 2005 and then worked as a postdoctoral research associate at the University of Illinois at Chicago and at the Condensed Matter Theory Center at the University of Maryland. His research focuses on low-dimensional systems, in particular 2D van der Waals systems and topological superconductors. He joined the



Laboratory.

Christopher Triola received his Ph.D. from William & Mary in 2015. He then worked as a postdoc at Nordita (2015–2017) and Uppsala University (2017–2019) studying primarily the electronic properties of Dirac materials, odd-frequency superconductivity, and the unconventional properties of driven solid state systems. Christopher is now a staff scientist at Los Alamos National

$a_{20} e^{-i(\theta_2 - \theta)}$, $\mathbf{a}_{22} = a_{20} e^{+i(\theta_2 + \theta)}$, where $a_{\ell 0}$ is the lattice constant of layer ℓ , $2\theta_\ell$ is the angle between the primitive lattice vectors of layer ℓ , and θ is the twist angle between the two layers. Using this notation, considering that the magnitudes of the two vectors on the left and right hand side of Equation (2) have to be same we obtain the following Diophantine equation constraining the integers m_1, m_2, n_1, n_2 :

$$\left(\frac{a_{10}}{a_{20}}\right)^2 (m_1^2 + m_2^2 + 2m_1 m_2 \cos 2\theta_1) = n_1^2 + n_2^2 + 2n_1 n_2 \cos 2\theta_2 \quad (3)$$

Notice that Equation (3) does not depend on θ . For a commensurate stacking the twist angle and the integers m_1, m_2, n_1, n_2 are related via the equation

$$\theta = \ln \left[\frac{a_{10}(m_1 e^{-i\theta_1} + m_2 e^{i\theta_1})}{a_{20}(n_1 e^{-i\theta_2} + n_2 e^{i\theta_2})} \right] \quad (4)$$

The number of commensurate stackings forms a set of measure zero in the whole space of possible stackings. However, the experimental evidence suggests^[42–46] that 2D vdW crystals tend to relax into stacking configurations that are, at least locally, commensurate.

The size of the primitive cell increases very rapidly as the twist angle θ decreases for $\theta < 5^\circ$. For this reason, to treat vdW systems with small twist angles, it is more efficient to use an

effective model in momentum space^[47–49] in which only the dominant interlayer tunneling processes are kept. For small twist angles an accurate description is obtained by keeping only those tunneling processes for which $|\mathbf{k}_1 - \mathbf{k}_2| = |\mathbf{G}_1 - \mathbf{G}_2|$ is smallest. For the practically important case in which the 2D crystals are triangular lattices and the low energy states (i.e., the states closest to the Fermi energy) are located at the corners (\mathbf{K} and \mathbf{K}' points) of the hexagonal Brillouin zone (BZ), as for graphene, the minimum value of $|\mathbf{G}_1 - \mathbf{G}_2|$ is equal to $2K \sin(\theta/2)$, where $K = |\mathbf{K}|$, and there are three vectors $\mathbf{q}_i = \mathbf{G}_1 - \mathbf{G}_2$ ($i = 1, 2, 3$) for which $|\mathbf{q}_i| = q = 2K \sin(\theta/2)$. If we account for all tunneling processes with $|\mathbf{k}_1 - \mathbf{k}_2| = q$ we find that the higher-order tunneling processes generate a honeycomb structure in momentum space with nearest neighbor points connected by the vectors \mathbf{q}_i .^[49]

The relative contributions of higher-order recursive tunneling processes is controlled by the parameter $\gamma \equiv t/(\epsilon(q))$, where t is the interlayer tunneling strength between states in the two layers with momenta that differ by at most q , and $\epsilon(q) = \min[\epsilon_1(q), \epsilon_2(q)]$, where $\epsilon_\ell(q)$ is the energy of electrons with momentum of magnitude q in layer ℓ . The value of γ , therefore, controls the size of this momentum space lattice that one needs to consider to obtain an accurate band structure for the vdW system. For $\gamma < 1$ the size of the required lattice in momentum space can be quite small. For very small γ it is sufficient to keep just the first “ring” of interlayer hopping processes. In this case the effective Hamiltonian matrix takes the simple form:

$$\hat{H}_{\mathbf{k}} = \begin{pmatrix} \hat{h}_1(\mathbf{k}) & \hat{t}_1^\dagger & \hat{t}_2^\dagger & \hat{t}_3^\dagger \\ \hat{t}_1 & \hat{h}_2(\mathbf{q}_1 + \mathbf{k}) & 0 & 0 \\ \hat{t}_2 & 0 & \hat{h}_2(\mathbf{q}_2 + \mathbf{k}) & 0 \\ \hat{t}_3 & 0 & 0 & \hat{h}_2(\mathbf{q}_3 + \mathbf{k}) \end{pmatrix} \quad (5)$$

where \hat{t}_i are matrices containing the interlayer tunneling elements.

The model described above can be generalized to the case when one (or more) of the layers forming the vdW system is superconducting. For concreteness, let us consider the case when the vdW system is formed by only two layers and only one is superconducting; it is fairly straightforward to generalize the formalism to more complex situations, such as when both layers are superconducting. We assume layer 2 is a superconductor so that $H_2 \rightarrow H_{SC}$, and that this superconducting layer is a 2D crystal with triangular lattice for which the low energy states are located close to the corners of the BZ, the \mathbf{K} and \mathbf{K}' points. We also assume simple s-wave pairing so that the superconducting order parameter Δ_{SC} couples states at opposite valleys with opposite spin and momentum \mathbf{k} , measured from \mathbf{K} (\mathbf{K}'). The Hamiltonian for the vdW system is $H = \sum_{\mathbf{k}} \Psi_{\mathbf{k}SC}^\dagger \hat{H}_{12}^{SC}(\mathbf{k}) \Psi_{\mathbf{k}SC}$, with $\Psi_{\mathbf{k}SC}^\dagger = (\psi_{\mathbf{k}}^\dagger, \psi_{-\mathbf{k}}^T)$,

$$\Psi_{\mathbf{k},\alpha,\beta_1,\beta_2,\beta_3}^\dagger = \left(c_{\mathbf{k},\alpha}^\dagger, d_{\mathbf{k}+\mathbf{q}_1,\alpha'}^\dagger, d_{\mathbf{k}+\mathbf{q}_2,\alpha'}^\dagger, d_{\mathbf{k}+\mathbf{q}_3,\alpha'}^\dagger \right) \quad (6)$$

and, to lowest order in γ :

$$\hat{H}_{12}^{SC}(\mathbf{k}) = \begin{pmatrix} \hat{h}_{12}(\mathbf{k}) & \hat{\Delta}_{SC} \hat{\Lambda} \\ \hat{\Delta}_{SC} \hat{\Lambda}^\dagger & -\hat{h}_{12}^T(-\mathbf{k}) \end{pmatrix} \quad (7)$$

where \hat{h}_{12} is the Hamiltonian given by Equation (5) and $\hat{\Lambda}$ is the matrix with indices describing the internal structure of the superconducting pairs in layer 2. For the case in which layer 1 has spin and sublattice degrees of freedom α and in layer 2, at low energies, we can assume that the only internal degree of freedom is the spin, $\hat{\Lambda}$ is a 10×10 block diagonal matrix given by:^[50]

$$\hat{\Lambda} = \text{diag}(0, i\hat{\sigma}_2, i\hat{\sigma}_2, i\hat{\sigma}_2) \quad (8)$$

where the first block is a 4×4 matrix of zeros and $\hat{\sigma}_2$ is a 2×2 Pauli matrix in spin space. As we will discuss in Section 5.2, the form for $\hat{\Lambda}$ given by Equation (8) is applicable to the case of a vdW structure composed of a superconducting TMD monolayer coupled to a graphenic layer, such SLG or BLG.

3. Graphene-TI Heterostructures

In this section we follow the theoretical treatment given in ref. [14] to examine the electronic properties of graphene-TI vdW heterostructures.^[51,52] The original motivation for studying the properties of a graphene layer coupled to the 2D surface of a 3DTI was the possibility of inducing strong SOC or novel spin textures in the graphene layer predicted by theoretical models.^[14,53,54] Excitingly, this proximity-induced SOC has recently been observed using a combination of transport measurements and ab initio calculations.^[15] Additionally, we also note that the possibility of inducing Dirac states with very low Fermi velocity, in which interaction effects could be greatly enhanced,^[55] has also been discussed.

In graphene the carbon atoms are arranged in a 2D honeycomb structure formed by two triangular sublattices, A and B , with lattice constant $a_g = \sqrt{3}a = 2.46\text{\AA}$, with $a = 1.42\text{\AA}$ the carbon-carbon atomic distance. The low energy states of graphene are located at the \mathbf{K} and \mathbf{K}' points of the BZ: $\mathbf{K} = (4\pi/(3a_g), 0)$, $\mathbf{K}' = (-4\pi/(3a_g), 0)$ (and equivalent points connected by reciprocal lattice wave vectors). At low energies close to the \mathbf{K} and \mathbf{K}' points in graphene, the electrons are well described as massless Dirac fermions with Hamiltonians

$$H_{\mathbf{k}}^{g,K} = \sum_{\mathbf{k}} \sum_{\tau\tau'} \sum_{\sigma\sigma'} c_{\mathbf{K}+\mathbf{k},\tau\sigma}^\dagger h_{\mathbf{k};\tau\tau',\sigma\sigma'}^{g,K} c_{\mathbf{K}+\mathbf{k},\tau'\sigma'} \quad (9)$$

$$\hat{h}_{\mathbf{k}}^{g,K} = (\hbar v_F \mathbf{k} \cdot \boldsymbol{\tau} - \mu_g \hat{\tau}_0) \otimes \hat{\sigma}_0$$

and

$$H_{\mathbf{k}}^{g,K'} = \sum_{\mathbf{k}} \sum_{\tau\tau'} \sum_{\sigma\sigma'} c_{\mathbf{K}'+\mathbf{k},\tau\sigma}^\dagger h_{\mathbf{k};\tau\tau',\sigma\sigma'}^{g,K'} c_{\mathbf{K}'+\mathbf{k},\tau'\sigma'} \quad (10)$$

$$\hat{h}_{\mathbf{k}}^{g,K'} = -(\hbar v_F \mathbf{k} \cdot \boldsymbol{\tau}^* + \mu_g \hat{\tau}_0) \otimes \hat{\sigma}_0$$

where $c_{\mathbf{p},\tau\sigma}^\dagger$ ($c_{\mathbf{p},\tau\sigma}$) is the creation (annihilation) operator for an electron, in the graphene sheet, with spin σ and 2D momentum $\hbar\mathbf{p} = \hbar(p_x, p_y)$, \mathbf{k} is a wave vector measured from \mathbf{K} (\mathbf{K}'), $v_F = 10^6 \text{ m s}^{-1}$ is the Fermi velocity, μ_g is the chemical potential, and $\hat{\tau}_i$ and $\hat{\sigma}_i$ ($i = 0, 1, 2, 3$) are the 2×2 Pauli matrices in sublattice and spin space, respectively.

One class of materials for which the effect of spin-orbit coupling on the low energy fermionic states is particularly strong is

one of the 3D topological insulators (TIs).^[11–13] In these materials the combination of spin-orbit coupling and time reversal symmetry guarantees the presence of topologically protected 2D surface states within the band gap of the bulk states. For this reason, 3D TI materials are in many respects ideal materials for the creation of novel vdW heterostructures in which the effect of SOC is significant.

The 2D states at the TI's surface (TIS) are well described as massless Dirac fermions with Hamiltonian:^[56,57]

$$H^{\text{TIS}} = \sum_{\mathbf{k}, \sigma \sigma'} d_{\mathbf{k}, \sigma}^\dagger h_{\mathbf{k}, \sigma \sigma'}^{\text{TIS}} d_{\mathbf{k}, \sigma'} \quad (11)$$

$$\hat{h}_{\mathbf{k}}^{\text{TIS}} = \hbar v_{\text{TI}} (\boldsymbol{\sigma} \times \mathbf{k}) \cdot \hat{\mathbf{z}} - \mu_{\text{TI}} \hat{\sigma}_0$$

where $d_{\mathbf{k}, \sigma}^\dagger$ ($d_{\mathbf{k}, \sigma}$) creates (annihilates) a surface massless Dirac fermion with spin σ at wave vector $\mathbf{k} = (k_x, k_y, 0)$ measured from the zone center ($\bar{\Gamma}$ -point) of the surface-projected (BZ), $\boldsymbol{\sigma} = (\hat{\sigma}_1, \hat{\sigma}_2, \hat{\sigma}_3)$ is the vector of Pauli matrices acting on spin space, $\hat{\mathbf{z}}$ is the unit vector in the z direction, and μ_{TI} is the chemical potential.

For our purposes, a particularly interesting class of 3D TIs is the one of the tetradymites, such as Bi_2Se_3 , Bi_2Te_3 , and Sb_2Te_3 . These 3D TIs have the exceptional property that the lattice constant of the 111 surface, a_{TI} , is such that: $a_{\text{TI}}/(\sqrt{3}a_g) = 1 + \delta$ with $\delta < 1\%$ for Sb_2Te_3 and $\delta \approx -3\%$ ($\delta \approx +3\%$) for Bi_2Se_3 (Bi_2Te_3).^[14] As a consequence, in the limit $\delta \rightarrow 0$, graphene and the TI surface can be stacked in a commensurate arrangement as shown, in momentum space, in **Figure 1a**. For such a stacking arrangement the corners of graphene's BZ are precisely above the $\bar{\Gamma}$ points of the TI surface BZ. For this stacking the primitive cell of the heterostructure corresponds to the primitive cell of the TI's surface and therefore the BZ of the resulting vdW system is equal to the BZ of the TI's surface. The K and K' points of the graphene BZ are folded back to the $\bar{\Gamma}$ point, as shown in **Figure 1b**.

In the remainder of this section we limit our discussion to the cases in which the TI is Bi_2Se_3 , Bi_2Te_3 , or Sb_2Te_3 , for which $v_{\text{TI}} \approx v_g/2$, given that these materials allow the formation of a graphene-TI vdW system with commensurate stacking and therefore significant hybridization between the graphene and TI

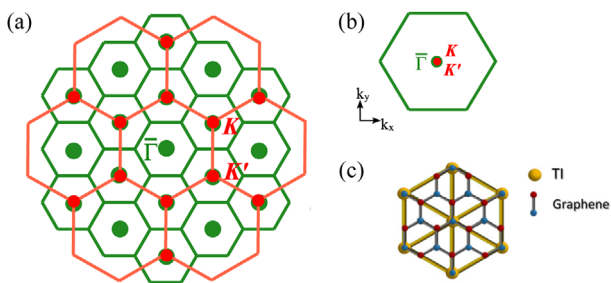


Figure 1. a) Schematic of the first seven extended Brillouin zones of graphene, shown in red, superimposed on the extended Brillouin zones of a TI, shown in green, for the case of $\sqrt{3} \times \sqrt{3}$ commensurate stacking. b) Depiction of the folded Brillouin zone for the same stacking as in (a). c) The real space picture associated with the $\sqrt{3} \times \sqrt{3}$ graphene-TI commensurate stacking. Adapted with permission from Phys. Rev. Lett. 112, 096802 (2014).

surface states. Experimentally it turns out to be difficult to pin the Fermi energy of Bi_2Se_3 , Bi_2Te_3 , Sb_2Te_3 in the middle of the bulk gap so that only the surface states play an active role. One way in which this problem has been overcome is by considering the corresponding ternary and quaternary compounds.^[58–64]

Different commensurate stacking configurations, corresponding to **Figure 1**, can be realized by rigid relative shifts of the graphene and TI lattices. Ab initio results^[53] suggest that the lowest energy stacking is the one for which the TI surface atoms are located at the center of the hexagons forming the graphene structure. However, the binding energy for the structure in which the TI surface atoms are directly below the carbon atoms of graphene (either the ones forming the A sublattice, or the ones forming the B sublattice) is only marginally higher.^[53] Considering that, experimentally, vdW systems are obtained via mechanical exfoliation that allows the realization of, long-lived, metastable states, and the fact that when the TI's surface atoms are directly below the carbon atoms of graphene a stronger hybridization of the graphene and TI states is realized, it is interesting to consider this situation.

In the $\sqrt{3} \times \sqrt{3}$ commensurate stacking, in which each atom on the TI surface is directly underneath a carbon atom, the dominant interlayer tunneling term is the one between the atoms on sublattice A (or B) and the TI atoms so that, in momentum space, the tunneling Hamiltonian can be written as $H_t = \sum_{\mathbf{k}, \lambda, \tau, \sigma} t_\tau d_{\mathbf{k}, \sigma}^\dagger c_{\lambda, \mathbf{k}, \tau, \sigma} + h.c.$, where $\lambda = K, K'$ and $t_A = t$, $t_B = 0$ are the tunneling matrix elements assumed to be spin and momentum independent. The Hamiltonian matrix for such a structure takes the form

$$\hat{H}_{\mathbf{k}} = \begin{pmatrix} \hat{h}_{\mathbf{k}}^{g, K} & 0 & \hat{t}^\dagger \\ 0 & \hat{h}_{\mathbf{k}}^{g, K'} & \hat{t}^\dagger \\ \hat{t} & \hat{t} & \hat{h}_{\mathbf{k}}^{\text{TIS}} \end{pmatrix}, \quad \hat{t} = \begin{pmatrix} t & 0 & 0 & 0 \\ 0 & 0 & t & 0 \end{pmatrix} \quad (12)$$

where the graphene blocks are 4×4 matrices in sublattice and spin space and the block describing the TI's surface states is a 2×2 matrix in spin space. We note that an analogous Hamiltonian can also be constructed for the similar vdW heterostructure in which single layer graphene (SLG) is replaced by bilayer graphene (BLG) to form a BLG-TI system.^[14]

The simple Hamiltonian in Equation (12) allows us to understand the qualitative features of the bands resulting from the hybridization between the graphene states and the states of the TI surface. **Figure 2a** shows the bands obtained by diagonalizing $\hat{H}_{\mathbf{k}}$ assuming $\mu_g = \mu_{\text{TI}} = 0$ and $t = 45$ meV. From **Figure 2a**, we see that the fourfold degeneracy of the graphene states (spin and valley degrees of freedom) is partially lifted as two spin-split Rashba bands appear (shown in red and blue). However, we also see that two of the original graphene states at the K and K' points remain spin degenerate (shown in grey), due to the fact that in the chosen configuration one sublattice does not couple to the TI. Moreover, the TI surface bands (shown in green) become quadratic at low energy as a consequence of hybridization with the graphene states.

We now discuss the case of stacking configurations that deviate from the $\sqrt{3} \times \sqrt{3}$ configurations discussed above either because of a small twist angle θ or because of a mismatch of the graphene and TI lattice constants. **Figure 3a,b** shows how the orientations

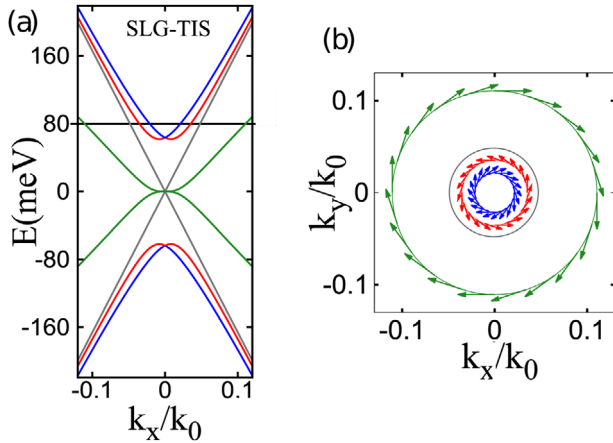


Figure 2. a) Band structure for the $\sqrt{3} \times \sqrt{3}$ commensurate graphene-TI structure described by Equation (12), assuming $\mu_g = \mu_{TI} = 0$ and $t = 45$ meV. b) The in-plane spin projection of the eigenstates associated with the bands in (a), evaluated at the energy $E = 80$ meV. Adapted with permission from Phys. Rev. Lett. 112, 096802 (2014).

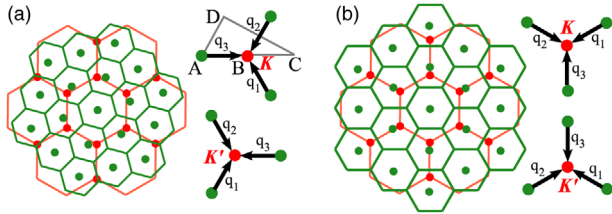


Figure 3. a) Schematic of the first seven extended Brillouin zones of graphene (red) superimposed on the extended Brillouin zones of a TI (green) with a slight rotation away from precise $\sqrt{3} \times \sqrt{3}$ commensurate stacking. Also shown the vectors q_i describing the displacement of the corners of the first Brillouin zone of graphene from the nearest $\bar{\Gamma}$ points in the TI surface. b) Similar schematic to (a) for the case when the deviation from the $\sqrt{3} \times \sqrt{3}$ commensurate stacking is caused by a lattice mismatch. Also shown the vectors q_i describing the displacement of the corners of the first Brillouin zone of graphene from the nearest $\bar{\Gamma}$ points in the TI surface for this case. Adapted with permission from Phys. Rev. Lett. 112, 096802 (2014).

of the TI and graphene BZs are affected by the presence of a twist angle and a lattice mismatch, respectively. We see that, due to the conservation of the crystal momentum, the states at the K (K') point of graphene now tunnel to the TI surface states with momentum q_i ($i = 1, 2, 3$). For the twisted case, the magnitude of this vector is $|q_j| \equiv q = 2K \sin(\theta/2)$, while for the case of a lattice mismatch we have $q = |\delta/(1 + \delta)|K$.

Assuming $\gamma \ll 1$, we can use the simple Hamiltonian in Equation (5), with $\hat{h}_1 = \hat{h}^{g,K}$, $\hat{h}_2 = h^{TI}$ and

$$\hat{t}_1 = \begin{pmatrix} t' & t' & 0 & 0 \\ 0 & 0 & t' & t' \end{pmatrix}, \quad \hat{t}_2 = \begin{pmatrix} t' & t' e^{-i\frac{2\pi}{3}} & 0 & 0 \\ 0 & 0 & t' & t' e^{-i\frac{2\pi}{3}} \end{pmatrix},$$

$$\hat{t}_3 = \begin{pmatrix} t' & t' e^{i\frac{2\pi}{3}} & 0 & 0 \\ 0 & 0 & t' & t' e^{i\frac{2\pi}{3}} \end{pmatrix}$$

with $t' = t/3$. A similar Hamiltonian is valid for the K' -valley.^[14] By diagonalizing the resulting Hamiltonian we obtain the low

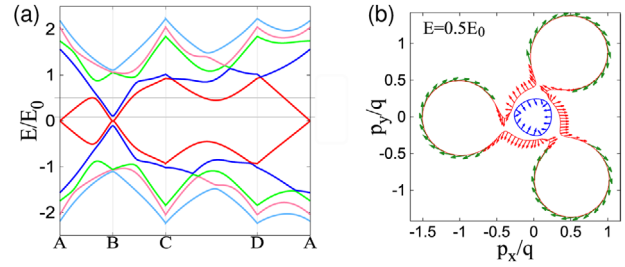


Figure 4. a) Band structure for a twisted graphene-TI system for the case when $\gamma = 0.2$, calculated by diagonalizing the Hamiltonian in Equation (5) along the ABCDA path indicated in Figure 3. b) The in-plane spin projection of the eigenstates associated with the bands in (a), evaluated at the energy $E = 0.5E_0$ where E_0 is indicated in (a). Adapted with permission from Phys. Rev. Lett. 112, 096802 (2014).

energy band structure. **Figure 4a** shows the bands along the path ABCDA shown in Figure 3a for the case when $\gamma = 0.2$. Assuming $t = 45$ meV, this value of γ corresponds to a deviation from the $\sqrt{3} \times \sqrt{3}$ stacking by a twist angle $\theta = 0.76^\circ$. **Figure 4b** shows the spin texture on the Fermi surface with $\epsilon_F = v_{TI}q/2$. Similar to the $\sqrt{3} \times \sqrt{3}$ commensurate case shown in **Figure 2**, we see that the strong SOC of the TI induces a strong spin polarization of the states of the hybridized system even when the stacking configuration deviates from the ideal $\sqrt{3} \times \sqrt{3}$ one.

3.1. Transport Properties

The intrinsic SOC in graphene and bilayer graphene is negligible so that the spin degree of freedom does not affect significantly the transport properties.^[7,65–72] In the presence of SOC, charge and spin transport become coupled.^[73–75] Therefore, in vdW systems with SOC we expect that, in general, transport properties will be spin-dependent and that such properties could differ considerably from isolated systems with SOC. Exemplary in this respect are the vdW systems formed by a layer with strong SOC, such as a TMD monolayer, and either graphene or bilayer graphene. In graphene-TI vdW systems the combination of the high mobility of graphene, the strong SOC of the TI, and the increased screening^[76–80] of impurities due to the presence of the graphene layer,^[81] can lead to very strong spin-dependent effects, such as a giant Edelstein effect.^[82] To illustrate the potential for realizing spin-dependent transport effects in vdW systems in which one layer has a strong SOC we discuss the case of a graphene-TI-Ferromagnet vdW system,^[82] shown schematically in **Figure 5a**.

Throughout this section, we assume that the ferromagnet (FM) is insulating so that its presence does not significantly alter the bands of the graphene-TI part of the vdW heterostructure. The main effect of the insulating FM layer is to induce an exchange field for the electrons in the heterostructure. This effect is captured by adding the term $H_{ex} \propto \mathbf{M} \cdot \boldsymbol{\sigma}$, where \mathbf{M} is the magnetization of the insulating FM, to the Hamiltonian discussed in Section 3. The presence of this additional term simply causes a spin-splitting that we denote by Δ .

In a graphene-TI-FM vdW system the dominant source of scattering, at low temperatures, is the presence of charge impurities^[83] close to the surface of the TI.^[84–88] In the absence of

screening, the bare scattering potential due to an isolated charge impurity, in momentum space, is $v(q) = 2\pi e^2 e^{-qd}/(\kappa q)$, where d is the average distance of the impurities from the TI's surface, and $\kappa = (\kappa_{TI} + \kappa_0)/2$ is the average dielectric constant with $\kappa_{TI} \approx 100$ ^[85,89–91] the dielectric constant for the TIS and $\kappa_0 = 1$ the dielectric constant of vacuum. Accounting for screening, the scattering potential becomes $v(q)/\epsilon(q)$ where $\epsilon(q)$ is the dielectric function. For temperatures much lower than the Fermi temperature we can assume $\epsilon(q) \approx 1 + v_c(q)v(\epsilon_F)$, where $v_c(q) = 2\pi e^2/(\kappa q)$ and $v(\epsilon_F)$ is the density of states at the Fermi energy. Using this form for the scattering potential we can calculate the lifetime $\tau_{0a}(\mathbf{k})$ of a quasiparticle in band a with momentum \mathbf{k} , in the first Born approximation, using

$$\frac{\hbar}{\tau_{0a}(\mathbf{k})} = 2\pi \sum_{a'q} n_{\text{imp}} \left| \frac{v(q)}{\epsilon(q)} \right|^2 |\langle a'\mathbf{k} + \mathbf{q} | a\mathbf{k} \rangle|^2 \delta(\epsilon_{a,\mathbf{k}} - \epsilon_{a',\mathbf{k}+\mathbf{q}}) \quad (13)$$

where n_{imp} is the impurity density, $|a\mathbf{k}\rangle$ is the Bloch state with momentum \mathbf{k} and band index a , and $\epsilon_{a,\mathbf{k}}$ is the energy for a quasiparticle with momentum \mathbf{k} in band a . For typical TI's samples we have $n_{\text{imp}} \approx 10^{12} \text{cm}^{-2}$.^[91] It is useful to define an average $\langle \tau_0 \rangle$ of τ_0 over the bands at the Fermi energy as $\langle \tau_0(\epsilon_F) \rangle \equiv \sum_{ka} \tau_{0a}(\mathbf{k}) \delta(\epsilon_F - \epsilon_{ka}) / \sum_{ka} \delta(\epsilon_F - \epsilon_{ka})$. We allow for an offset between the charge neutrality point of the SLG (BLG) and the TI surface given by $\delta\mu$.

Figure 5b shows how $\langle \tau_0(\epsilon_F) \rangle$ compares for: an isolated TI surface, a SLG-TI vdW system, and BLG-TI vdW system. Solid lines denote the cases when the tunneling between the SLG/BLG and the TI is finite, while dashed lines denote the cases with zero interlayer coupling. We see that the presence of SLG or BLG significantly increases the quasiparticle lifetime, even in the limit when the interlayer tunneling between the TI and SLG (BLG) is zero. This is due to the additional screening in the presence of SLG or BLG which affects the disorder potential created by the charge impurities.^[81,92] We expect that such an increase in the quasiparticle lifetime will lead to enhancements in some of the spin-dependent transport phenomena. Similarly, by including the $[1 - \mathbf{k} \cdot (\mathbf{k} + \mathbf{q})]$ under the sum on the right hand side of Equation (13) we can obtain the transport time $\tau_{ia}(\mathbf{k})$, and then, after averaging over the bands at the Fermi energy, the corresponding average $\langle \tau_i \rangle$. Figure 6a shows $\langle \tau_i \rangle$ as a function of ϵ_F for an isolated TI surface together with results for, both, TI-SLG, and TI-BLG vdW systems. We see that the presence of SLG or BLG increases the transport time, a consequence of the additional

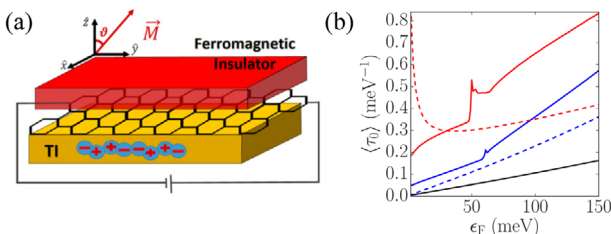


Figure 5. a) Sketch of a TI-graphene-FM vdW system. b) $\langle \tau_0(\epsilon_F) \rangle$ for $\Delta = 0$, $\delta\mu = 0$, $n_{\text{imp}} = 10^{12} \text{cm}^{-2}$, and $d = 1 \text{nm}$. The dashed lines show the results for the limit $t = 0$, the solid one the ones for $t = 45 \text{meV}$. Adapted with permission from Phys. Rev. B **96**, 235419 (2017).

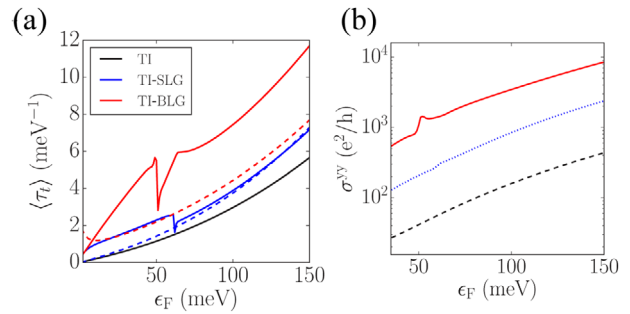


Figure 6. a) $\langle \tau_i(\epsilon_F) \rangle$ for $\Delta = 0$, $\delta\mu = 0$, and $n_{\text{imp}} = 10^{12} \text{cm}^{-2}$. The dashed lines show the results for the limit $t = 0$, the solid one the ones for $t = 45 \text{meV}$. b) $\sigma^{yy}(\epsilon_F)$, for TI (dashed line), TI-SLG (dotted line), and TI-BLG (solid line) for $\Delta = 0$, $\delta\mu = 0$, $n_{\text{imp}} = 10^{12} \text{cm}^{-2}$, $d = 1 \text{nm}$, and $t = 45 \text{meV}$, and Adapted with permission from Phys. Rev. B **96**, 235419 (2017).

screening due to the graphenic layer. Moreover, we note that this enhancement is particularly significant for the case of TI-BLG.

Using linear-response theory in the long-wavelength regime, the d.c. longitudinal conductivity is given by

$$\sigma^{ii} \approx \frac{e^2}{2\pi\Omega} \text{Re} \sum_{k,a} v_{aa}^i(\mathbf{k}) \tilde{v}_{aa}^i(\mathbf{k}) G_{ka}^A G_{ka}^R \quad (14)$$

where Ω is the area of the BZ, $v_{aa}^i(\mathbf{k}) \equiv \langle a\mathbf{k} | v_i | a\mathbf{k} \rangle$ is the expectation value of the i -th component of the velocity operator $\mathbf{v} = \hbar^{-1} \partial H_k / \partial \mathbf{k}$, $\tilde{v}_{aa}^i(\mathbf{k}) = (\tau_a / \tau_{0a})_k v_{aa}^i(\mathbf{k})$ is the disorder-renormalized velocity (at the ladder approximation level), and $G_{ka}^{R/A} = (\epsilon_F - \epsilon_{ka} \pm i\hbar/2\tau_{0a}(\mathbf{k}))^{-1}$ is the retarded/advanced Green's function, for electrons with momentum \mathbf{k} and band index a . The increase of τ_i due to the presence of SLG or BLG is also reflected in an increase of the d.c. conductivity, as can be seen in Figure 6b. We note that for finite values of the spin-splitting, Δ , the results for τ_0 , τ_i , and σ^{ii} are very similar to the ones shown in Figures 5b and 6.^[82]

Having established the basic charge transport properties we now briefly discuss spin-dependent transport. A signature effect of the coupling between charge and spin transport that can take place in systems with spin-orbit coupling is the inverse Edelstein effect.^[93,94] In this effect a charge current causes a spin accumulation transverse to the direction of the current. In the long wavelength, dc, limit, of the linear response regime, such an effect is encoded by the spin-current response function:

$$\chi^{s_x j_y} \approx \frac{e}{2\pi\Omega} \text{Re} \sum_{k,a} s_{aa}^x(\mathbf{k}) \tilde{v}_{aa}^y(\mathbf{k}) G_{ka}^A G_{ka}^R \quad (15)$$

where $s_{aa}^i(\mathbf{k}) \equiv \langle a\mathbf{k} | s_i | a\mathbf{k} \rangle$ is the expectation value of the i -th component of the spin density operator.

Figure 7a displays a significant enhancement of the spin-current response $\chi^{s_x j_y}$ in SLG-TI (BLG-TI) vdW system, compared to an isolated TI's surface. This enhancement is due to the presence of the graphenic layer and occurs for, both, the case of finite (solid lines) and zero Δ (dashed lines). As the sketch in the inset shows, a current in the y -direction causes a spin accumulation in the transverse direction x . An increase of $\delta\mu$ can significantly enhance the spin-current response, as shown in Figure 7b, whereas Δ has a small effect.^[82]

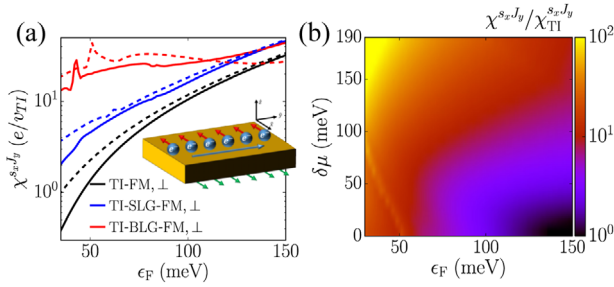


Figure 7. a) $\chi^{s_x s_y}$ as a function of ϵ_F for $\delta\mu = 0$ and $\Delta = 20$ meV ($\Delta = 0$), solid (dashed) lines. Inset: sketch showing the spin density accumulation on the top and bottom surface of the TI induced by a current in the y direction. b) Enhancement of $\chi^{s_x s_y}$ in a TI-BLG system compared to TI alone as a function of ϵ_F and $\delta\mu$ for $\Delta = 0$. For both the panels $n_{\text{imp}} = 10^{12} \text{ cm}^{-2}$, $d = 1$ nm. Adapted with permission from Phys. Rev. B **96**, 235419 (2017).

The fact that the Edelstein effect can be much stronger in vdW systems like TI-SLG and TI-BLG than in isolated TIs^[95–100] is due to the fact that the bands for the vdW system retain a strong SOC, even after the hybridization of the states in the TI and the graphenic layer, and the fact that the quasiparticle relaxation time can be greatly increased when the dominant source of scattering is charge impurities, thanks to the additional screening provided by the graphenic layer. As mentioned above, the enhancement of the lifetime gained from the additional screening makes it possible for vdW systems like TI-BLG to have quite stronger spin-charge coupled transport than isolated systems like TIs even when the tunneling between the two layers of the vdW system is negligible.

So far we have considered the case in which the interlayer tunneling is constant; however, spin and charge transport can be coupled in vdW systems such as graphene-TI heterostructures even in the limit when the interlayer tunneling is predominantly random.^[101] In this case the evolution, in the diffusive limit, of the graphene's charge density, n , and spin density, \mathbf{s} , are given by the following equations:^[101]

$$\partial_t n = \bar{D} \nabla^2 (n + 2\rho V) + \Gamma_{ns} l_{\text{TI}} (\hat{z} \times \nabla) (\mathbf{s} - 2\rho \mathbf{h}) - 2 \frac{\rho \Gamma^t}{\Gamma^t + \Gamma_{\text{TI}}^t} \partial_t (V - V_{\text{TI}}) \quad (16)$$

$$\partial_t \mathbf{s} = (D \nabla^2 - \Gamma^t) (\mathbf{s} - 2\rho \mathbf{h}) + \alpha \Gamma^t l_{\text{TI}} (\hat{z} \times \nabla) \times (\mathbf{s} - 2\rho \mathbf{h}) + \Gamma^t l_{\text{TI}} (\hat{z} \times \nabla) [l_{\text{TI}} (\nabla \times (\mathbf{s} - 2\rho \mathbf{h}))_z + (n + 2\rho V)/2] \quad (17)$$

where V , V_{TI} are external driving potentials for the charge in the graphene layer and TI's surface, respectively, ρ is graphene's density of states at the Fermi energy, and \mathbf{h} is an external driving potential for the spin in the graphene layer. \bar{D} is the weighted average of the diffusion constants of graphene, D , and TI's surface, D_{TI}

$$\bar{D} = \frac{\Gamma^t D_{\text{TI}} + \Gamma_{\text{TI}}^t D}{\Gamma^t + \Gamma_{\text{TI}}^t}$$

where Γ^t , Γ_{TI}^t , are the tunneling rates for graphene and the TI, respectively: $\Gamma^t = \pi \rho_{\text{TI}} t^2$, $\Gamma_{\text{TI}}^t = \pi \rho t^2$, with ρ_{TI} the density of states

of the TI's surface at the Fermi energy. The interlayer tunneling processes are assumed to be well localized in space so that in momentum space the disorder average of the second moment of the interlayer tunneling matrix is just a constant, t^2 . The second term on the right hand side (r.h.s.) of Equation (16) describes the coupling between charge and spin transport with

$$\Gamma_{ns} = 2 \frac{\Gamma^t \Gamma_{\text{TI}}^t}{\Gamma^t + \Gamma_{\text{TI}}^t}$$

and l_{TI} the electron's mean free path on the TI's surface. The last term on the r.h.s. of Equation (16) describes the effect of time-dependent driving potentials for the charge. The second term on the r.h.s. of Equation (17) is due to the spin-orbit coupling term that is induced by proximity in the layer with no spin-orbit coupling even when the interlayer tunneling is predominantly random. The coefficient of this term is

$$\alpha = \frac{\epsilon_F \tau^0}{2\pi^2 \rho_{\text{TI}} D_{\text{TI}}}$$

where ϵ_F is the Fermi energy and τ^0 is the quasiparticle relaxation time in the graphene layer due to intralayer disorder.

Equations (16) and (17) are valid when the interlayer tunneling rate is much smaller than the intralayer scattering rate, and for time scales much longer than the largest relaxation time τ ($\omega\tau \ll 1$). They show that even when the interlayer tunneling is random, charge and spin transport in the layer with no SOC are coupled. We can then conclude that even for vdW systems in which, due to the low quality of the interfaces, the interlayer tunneling is random, spintronics effects, such as the Edelstein effect, can be realized.^[101] The fact that Γ_{ns} depends on the intralayer and interlayer scattering rates, that in turn are directly proportional to the density of states at the Fermi energy, implies that in systems in which for at least one of the layers the density of states depends on the doping –such as for the surface of a TI or graphene– it is possible to tune the coupling between spin and charge transport simply via external gate voltages.

4. Graphene-TMD Heterostructures

In recent years, much progress has been made on the characterization of the electronic properties of graphene-TMD heterostructures, both theoretically and experimentally. A monolayer TMD can be either metallic, such as NbSe₂, or a direct gap semiconductor such as MoS₂, and WSe₂. At low temperatures NbSe₂ becomes superconducting and so we defer discussion of graphene-NbSe₂ vdW systems to the following section, see in particular Section 5.2. In this section we briefly summarize the main results for graphene-TMD heterostructures in which the TMD is a semiconductor.

The structure of a TMD monolayer is shown schematically in Figure 8a where the purple spheres represent the metallic atoms, such as Mo in MoS₂, and the green spheres the chalcogen atoms, S in MoS₂. One of the main features of TMDs is the presence of strong SOC, which, in monolayers, induces a sizeable spin splitting of the hole bands^[102–106] located at the corners of the BZ, as shown in Figure 8b. At low energies, the bands of a TMD

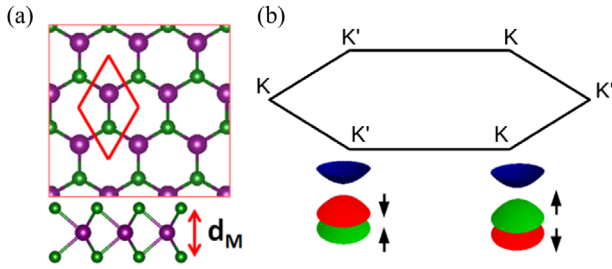


Figure 8. a) Sketch of the typical lattice of a transition metal dichalcogenide monolayer, with purple spheres representing the metallic atoms and green spheres the chalcogen atoms. b) Schematic of the first Brillouin zone of MoS₂ with the low energy bands at the K and K' points. Spin-polarization of the valence bands denoted with arrows. Adapted with permission from Phys. Rev. Lett. 116, 257001 (2016).

semiconductor monolayer such as MoS₂, are well described by the following Hamiltonian:^[107]

$$\hat{h}_k^{TMD} = a\gamma (\lambda k_x \hat{k}_1 + k_y \hat{k}_2) + \frac{u}{2} \hat{k}_3 - \mu \hat{k}_0 - \frac{\lambda\alpha}{2} (\hat{k}_3 - \hat{k}_0) \otimes \hat{\sigma}_3 \quad (18)$$

where a is the in-plane lattice constant, γ the in-plane hopping amplitude, $\lambda = \pm 1$ is the index denoting the valley (K or K'), k_x, k_y are the in-plane components of the electrons wave vector, measured from the corner of the BZ, \hat{k}_i are 2×2 Pauli matrices in the orbital space,^[102] u is the band-gap, μ the chemical potential, and 2α is the spin-splitting of the valence bands at the K (K') point due to the presence of spin-orbit coupling. In the case of MoS₂ these parameters are $a = 3.193\text{\AA}$, $\gamma \approx 1.1$ eV, $u \approx 1.65$ eV, and $2\alpha \approx 0.15$ eV.^[102]

Given that the semiconducting monolayer TMDs have a fairly large gap, ≈ 2 eV, and a large lattice mismatch with graphene, one would expect that their effect on the graphene band structure could be negligible. Indeed, it is the case that the effects induced by proximity of the TMD to the SLG (or BLG) are quantitatively small. However, the presence of these effects can be qualitatively very significant due to the fact that in pristine SLG and BLG the spin-splitting from intrinsic SOC is very small, of the order of $10 \mu\text{eV}$.^[108] This means that even a small enhancement of the SOC induced by the proximity of a TMD monolayer can profoundly affect the electronic properties of SLG and BLG.

Ab initio calculations^[109–111] show that semiconducting monolayer TMDs such as MoS₂, MoSe₂, MoTe₂, WS₂, WSe₂, WTe₂ can enhance SOC in graphene to induce spin-splittings of the order of 1 meV, that is, orders of magnitude larger than the graphene's intrinsic SOC. The enhancement increases with the atomic number of the metal forming the TMD. For the case of graphene-WSe₂vdW systems the SOC induced by proximity in graphene is sufficient to create a band inversion of the spin-split bands close to the original graphene's Dirac point. Such a band inversion could lead to topological phases exhibiting the quantum spin Hall effect in SLG-TMD^[110,112,113] or BLG-TMD^[114] heterostructures. The enhancement of the SOC in graphene-TMD vdW systems has been observed, indirectly, via weak antilocalization^[115–121] and spin-relaxation measurements.^[122–126] It has also been suggested that by tuning the twist angle between graphene and the TMD the nature, from Zeeman-like to Rashba-like, and strength of the induced SOC can be tuned.^[127,128] Similarly to the case of

graphene-TI systems, spin and charge transport are also coupled in graphene-TMD heterostructures^[129,130] as demonstrated experimentally in graphene-MoS₂,^[131,132] graphene-WS₂,^[133,134] graphene-MoTe₂,^[135] and graphene-TaS₂.^[136] devices.

For the case of TMD-BLG vdW systems the resulting structure of the hybridized bands is richer and tunable via an external electric field.^[111] For WSe₂-BLG ab initio results show that the proximity of the TMD induces a gap in BLG of the order of 10 meV and SOC splittings of about 2 meV.^[111] Very recent experiments^[137] on symmetric WSe₂-BLG-WSe₂vdW systems have shown a strong enhancement of the SOC in graphene and clear signatures of the SOC-driven band inversion.

5. Superconductor-Based van der Waals Systems

Van der Waals heterostructures constructed with superconducting layers are extremely interesting because they allow the realization of novel superconducting states. In particular, when one of the layers has strong SOC, such heterostructures can be engineered to realize topologically non-trivial superconducting states^[138–142] as well as states with odd-frequency pairing.^[143,144] Given the scope of the special issue, below we focus on the cases in which the vdW heterostructure can host odd-frequency superconducting pairing.

5.1. Odd-Frequency Pairing

In general, the order parameter describing a correlated electronic state is given by a many-body wavefunction, which must be completely antisymmetric under the permutation of all quantum numbers. This antisymmetry constrains the allowed symmetries of the order parameter. In the limit of static order parameters and a single relevant band degree of freedom, this constraint implies that even-parity order parameters (s - or d -wave) must be odd in the spin index (spin-singlet) while odd-parity order parameters (p - or f -wave) must be even in spin (spin-triplet). The term odd-frequency pairing refers to the possibility that the many-body state is odd in the relative time coordinate, or, equivalently, in the relative frequency. Therefore, odd-frequency states must possess spatial and spin symmetries with the exact opposite correspondence from the static case: that is, even-parity states must be spin-triplet and odd-parity must be spin-singlet. An odd-frequency state was first proposed by Berezinskii^[145] as a possible superfluid state for He³. Later on, Berezinskii's proposal was extended to superconducting systems.^[146–151] However, it has been pointed out that constraints on the electron-phonon interactions inhibit odd-frequency pairing,^[152] and that simple models of intrinsically odd-frequency superconducting states may be unstable.^[153–155]

While the status of intrinsic odd-frequency states is uncertain, much progress has been made toward understanding how odd-frequency superconducting correlations can be induced using conventional superconductors in heterostructures. One theoretically well-established example can be found in superconductor-ferromagnet junctions which allow the conversion of conventional s -wave spin-singlet Cooper pairs to odd-frequency spin-triplet pairs, due to the breaking of spin-rotational

symmetry.^[143,156–163] Experimental signatures of odd-frequency correlations have been observed in real systems.^[164–170] Another notable example is the interface between a conventional superconductor and a normal metal, in which odd-frequency pairing can emerge due to broken spatial translation symmetry.^[171,172] In this case, the magnitudes of the odd-frequency correlations dominate over the even-frequency amplitudes at discrete energy levels coinciding exactly with peaks in the local density of states,^[172] indicating a relationship between these odd-frequency pair amplitudes and McMillan–Rowell oscillations^[173,174] as well as midgap Andreev resonances.^[175–177] Similar phenomena have also been predicted to arise in layered 2D systems, like vdW heterostructures, in which one of the components is superconducting.^[16,178–185] Given the growing number of vdW systems available, the high level of tunability of their properties, and the presence of a 2D surface accessible for interrogation by experiments, vdW systems are ideal candidates for studying odd-frequency superconducting states.

A set of general criteria for the emergence of odd-frequency pairing in 2D systems were given in ref. [16]. To understand how their results relate to layered vdW systems we will now provide a sketch of their derivation.

To begin, we consider a vdW system formed by a 2D crystal with Hamiltonian H_{2D} , and a superconductor with Hamiltonian H_{SC} . Without loss of generality we assume the superconductor to also be 2D. Let H_t describe tunneling processes between the 2D and the SC so that the Hamiltonian H for the entire bilayer system can be written as $H = H_{2D} + H_{SC} + H_t$, with

$$H_{2D} = \sum_{\mathbf{k}, \sigma, \sigma'} c_{\mathbf{k}, \sigma}^\dagger [h_0(\mathbf{k}) \hat{\sigma}_0 + \mathbf{h}(\mathbf{k}) \cdot \boldsymbol{\sigma}]_{\sigma, \sigma'} c_{\mathbf{k}, \sigma'} \quad (19)$$

$$H_{SC} = \sum_{\mathbf{k}, \sigma, \sigma'} d_{\mathbf{k}, \sigma}^\dagger h_{\sigma\sigma'}^{SC}(\mathbf{k}) d_{\mathbf{k}, \sigma'} + \sum_{\mathbf{k}, \sigma, \sigma'} d_{\mathbf{k}, \sigma}^\dagger \Delta_{\sigma\sigma'}(\mathbf{k}) d_{-\mathbf{k}, \sigma'}^\dagger + \text{h.c.} \quad (20)$$

$$H_t = t \sum_{\mathbf{k}, \sigma} d_{\mathbf{k}, \sigma}^\dagger c_{\mathbf{k}, \sigma} + \text{h.c.} \quad (21)$$

where $\hat{\sigma}_i$ are the 2×2 Pauli matrices in spin space, $c_{\mathbf{k}, \sigma}^\dagger$ ($d_{\mathbf{k}, \sigma}^\dagger$) and $c_{\mathbf{k}, \sigma}$ ($d_{\mathbf{k}, \sigma}$) are the creation and annihilation operators, respectively, acting on the fermionic states in the 2DEG (SC) layer with momentum \mathbf{k} and spin σ , $h_0(\mathbf{k})$ is the spin-independent part of H_{2D} and $\mathbf{h}(\mathbf{k})$ is the field that describes its spin-dependent part due to an exchange field and/or spin-orbit coupling. Here, $h_{\sigma\sigma'}^{SC}(\mathbf{k})$ describes the quasiparticle spectrum of the normal state of the superconductor, $\Delta_{\sigma\sigma'}(\mathbf{k})$ is the superconducting order parameter which, in general, has a linear combination of spin-singlet and spin-triplet terms, and t is the tunneling between the 2D system and the SC, which is assumed to conserve both spin and momentum.

To examine the superconducting pairing induced in the non-superconducting 2DEG by proximity to the SC, we study the anomalous Green's function, or pair amplitude, within the 2DEG, $\hat{F}_{\mathbf{k}; i\omega_n}^{2D}$, which is a 2×2 matrix in spin space and a function of both the crystal momentum \mathbf{k} and Matsubara frequency ω_n . In the absence of interlayer tunneling t no superconducting pairs exist in the 2DEG and therefore $\hat{F}_{\mathbf{k}; i\omega_n}^{2D} = 0$. However, for $t \neq 0$ we find that Cooper pairs can tunnel from the SC into the 2DEG, giving rise to superconducting correlations with novel symmetries

which depend on the properties of the 2DEG. To understand the symmetries of these induced pairings it is sufficient to consider the leading-order terms in perturbation with respect to the tunneling strength t :

$$\hat{F}_{\mathbf{k}; i\omega_n}^{2D} = t^2 \hat{G}_{\mathbf{k}; i\omega_n}^{2D} \hat{F}_{\mathbf{k}; i\omega_n}^{SC} \left(\hat{G}_{-\mathbf{k}; -i\omega_n}^{2D} \right)^T \quad (22)$$

where $\hat{F}_{\mathbf{k}; i\omega_n}^{SC}$ is the anomalous part of the Green's function for the SC, given by

$$\hat{F}_{\mathbf{k}; i\omega_n}^{SC} = \left(s_{\mathbf{k}; i\omega_n}^{SC} \hat{\sigma}_0 + \mathbf{d}_{\mathbf{k}; i\omega_n} \cdot \boldsymbol{\sigma} \right) i\hat{\sigma}_2 \quad (23)$$

where $s_{\mathbf{k}; i\omega_n}^{SC}$ ($\mathbf{d}_{\mathbf{k}; i\omega_n}$) represents the spin-singlet (spin-triplet) pair amplitudes and $\hat{G}_{\mathbf{k}; i\omega_n}^{2D}$ is the normal Green's function for the 2DEG when $t = 0$, given by

$$\hat{G}_{\mathbf{k}; i\omega_n}^{2D} = \frac{(i\omega_n - h_0(\mathbf{k})) \hat{\sigma}_0 + \mathbf{h}(\mathbf{k}) \cdot \boldsymbol{\sigma}}{(i\omega_n - h_0(\mathbf{k}))^2 - |\mathbf{h}(\mathbf{k})|^2} \quad (24)$$

Inserting Equations (23) and (24) into Equation (22) we obtain the expression for $\hat{F}_{\mathbf{k}; i\omega_n}^{2D}$, which can be written as

$$\hat{F}_{\mathbf{k}; i\omega_n}^{2D} = A_{\mathbf{k}; i\omega_n} \left(F_{\mathbf{k}; i\omega_n}^{odd} + F_{\mathbf{k}; i\omega_n}^{even} \right) \quad (25)$$

where $F_{\mathbf{k}; i\omega_n}^{even}$ ($F_{\mathbf{k}; i\omega_n}^{odd}$) are strictly even (odd) functions of Matsubara frequency ω_n , and

$$A_{\mathbf{k}; i\omega_n} = t^2 \left[\left[(i\omega_n + h_0(-\mathbf{k}))^2 - |\mathbf{h}(-\mathbf{k})|^2 \right]^{-1} \times \left[(i\omega_n - h_0(\mathbf{k}))^2 - |\mathbf{h}(\mathbf{k})|^2 \right]^{-1} \right] \quad (26)$$

is the spin-independent amplitude arising from the product of the denominators of the Green's functions $\hat{G}_{\mathbf{k}; i\omega_n}^{2D}$, $\hat{G}_{-\mathbf{k}; -i\omega_n}^{2D}$. For the most general form of H_{2D} , $A_{\mathbf{k}; i\omega_n}$ has both even and odd-frequency terms; however, assuming $h_0(\mathbf{k}) = h_0(-\mathbf{k})$ and $|\mathbf{h}(\mathbf{k})| = |\mathbf{h}(-\mathbf{k})|$, which are true for most systems, $A_{\mathbf{k}; i\omega_n}$ becomes an even function of both frequency and momentum. In this case the relative contributions from the even- and odd-frequency pair amplitudes are given by $F_{\mathbf{k}; i\omega_n}^{even}$ and $F_{\mathbf{k}; i\omega_n}^{odd}$, respectively.

We can decompose each of these even/odd-frequency amplitudes into spin-singlet and spin-triplet components:

$$F_{\mathbf{k}; i\omega_n}^{even} = \left(S_{\mathbf{k}; i\omega_n}^{even} \hat{\sigma}_0 + \mathbf{D}_{\mathbf{k}; i\omega_n}^{even} \cdot \boldsymbol{\sigma} \right) i\hat{\sigma}_2 \quad (27)$$

$$F_{\mathbf{k}; i\omega_n}^{odd} = i\omega_n \left(S_{\mathbf{k}; i\omega_n}^{odd} \hat{\sigma}_0 + \mathbf{D}_{\mathbf{k}; i\omega_n}^{odd} \cdot \boldsymbol{\sigma} \right) i\hat{\sigma}_2 \quad (28)$$

where, for the even-frequency amplitudes we have:

$$S_{\mathbf{k}; i\omega_n}^{even} = \left[\omega_n^2 + h_0^2(\mathbf{k}) - \frac{1}{4} (|\mathbf{h}_+(\mathbf{k})|^2 - |\mathbf{h}_-(\mathbf{k})|^2) \right] s_{\mathbf{k}; i\omega_n}^{SC} - \left[h_0(\mathbf{k}) \mathbf{h}_-(\mathbf{k}) + \frac{i}{2} \mathbf{h}_+(\mathbf{k}) \times \mathbf{h}_-(\mathbf{k}) \right] \cdot \mathbf{d}_{\mathbf{k}; i\omega_n} \quad (29)$$

$$\begin{aligned} D_{k;io}^{even} = & \left[\omega_n^2 + h_0^2(\mathbf{k}) + \frac{1}{4}(|\mathbf{h}_+(\mathbf{k})|^2 - |\mathbf{h}_-(\mathbf{k})|^2) \right] \mathbf{d}_{k;io_n} \\ & - i h_0(\mathbf{k}) \mathbf{h}_+(\mathbf{k}) \times \mathbf{d}_{k;io_n} - \frac{1}{2} \mathbf{h}_+(\mathbf{k}) (\mathbf{h}_+(\mathbf{k}) \cdot \mathbf{d}_{k;io_n}) \\ & + \frac{1}{2} \mathbf{h}_-(\mathbf{k}) (\mathbf{h}_-(\mathbf{k}) \cdot \mathbf{d}_{k;io_n}) \\ & - \left[h_0(\mathbf{k}) \mathbf{h}_-(\mathbf{k}) - \frac{i}{2} \mathbf{h}_+(\mathbf{k}) \times \mathbf{h}_-(\mathbf{k}) \right] s_{k;io_n}^{SC} \end{aligned} \quad (30)$$

and for the odd-frequency amplitudes:

$$S_{k;io_n}^{odd} = -\mathbf{h}_+(\mathbf{k}) \cdot \mathbf{d}_{k;io_n} \quad (31)$$

$$D_{k;io}^{odd} = -\mathbf{h}_+(\mathbf{k}) s_{k;io_n}^{SC} - i \mathbf{h}_-(\mathbf{k}) \times \mathbf{d}_{k;io_n} \quad (32)$$

where $\mathbf{h}_\pm(\mathbf{k}) \equiv \mathbf{h}(\mathbf{k}) \pm \mathbf{h}(-\mathbf{k})$ is the even/odd parity part of the spin-dependent field in the 2DEG. Here, \mathbf{h}_+ can be interpreted as the field arising from ferromagnetic ordering and \mathbf{h}_- as the field due to SOC.

Focusing first on the even-frequency spin-singlet amplitudes, we note that the first line in Equation (29) shows that, as expected, if the SC layer has spin-singlet pair amplitudes, spin-singlet pairing is also induced in the 2DEG. Moreover, from the second line of Equation (29) we see that, due to the presence of SOC in the 2DEG, a singlet term can also be induced by spin-triplet pairing in the SC. It is interesting to note that such contributions are only possible if $\mathbf{h}_- \neq 0$ and can be enhanced by adjusting the angle between $\mathbf{h}_+(\mathbf{k})$ and $\mathbf{h}_-(\mathbf{k})$.

Turning our attention to the induced even-frequency spin-triplet pairing, we see that the first line in Equation (30) shows an induced triplet pairing in the 2DEG directly proportional to the \mathbf{d} vector in the SC, as expected. The second and third lines in Equation (30) show that the presence of the spin-dependent $\mathbf{h}(\mathbf{k})$ field in the 2DEG layer induces a rotation of the \mathbf{d} vector. The last line in Equation (30) shows that the presence of SOC in the 2DEG layer also converts some of the spin-singlet amplitudes in the SC to spin-triplet pairing in the 2DEG. As in Equation (29), we only find this symmetry conversion between triplet and singlet amplitudes when $\mathbf{h}_- \neq 0$.

We now focus on the induced odd-frequency amplitudes. From Equation (31) we see that an odd-frequency spin-singlet amplitude is induced in the 2DEG layer when $\mathbf{h}_+(\mathbf{k}) \neq 0$ and a triplet component is present in the SC. In contrast to the case of induced even-frequency spin-singlet pairing, this odd-frequency amplitude emerges due to a conversion of spin-triplet amplitude in the SC to spin-singlet amplitude in the 2DEG for finite $\mathbf{h}_+(\mathbf{k})$ not $\mathbf{h}_-(\mathbf{k})$.

In the case of the odd-frequency spin-triplet pairing, Equation (32) shows that two contributions are possible. One of these involves a conversion from spin-singlet pairing in the SC to triplet pairing in the 2DEG when $\mathbf{h}_+(\mathbf{k}) \neq 0$. We note that this term, and Equation (31) are consistent with known results for the case of ferromagnet/superconductor junctions.^[143,156–163,186] The last term in Equation (32) shows that a triplet component in the SC can also induce an odd-frequency triplet term in the 2DEG in the presence of SOC, $\mathbf{h}_-(\mathbf{k}) \neq 0$, as long as \mathbf{h}_- is not parallel to \mathbf{d}_k . Typically, for an isolated system, the superconducting \mathbf{d}_k vector is parallel to the direction of the SOC field and so the presence of

triplet pairing and SOC is not sufficient to realize odd-frequency pairing. However, in a vdW, due to the fact that the vector fields $\mathbf{h}_-(\mathbf{k})$ and \mathbf{d}_k live in different layers, the condition $\mathbf{h}_-(\mathbf{k}) \times \mathbf{d}_k$ can be readily realized, as demonstrated in the concrete example below. This fact, also considering the great experimental advances in creating high quality vdW systems comprising a large variety of materials, considerably enlarges the set of systems in which odd-frequency superconducting pairing can be realized and detected.

A real system in which the condition $\mathbf{h}_-(\mathbf{k}) \times \mathbf{d}_k \neq 0$ can be realized is a vdW system formed by a monolayer transition metal dichalcogenide (TMD) placed on a superconducting surface with Rashba SOC.^[16] Considering only states close to the valence bands in the TMD layer, the Hamiltonian in Equation (18) can be simplified to obtain:

$$\hat{h}_{k,\lambda}^{TMD} = -\left(\frac{a^2 \gamma^2}{u} k^2 + \frac{u}{2} + \mu \right) + \lambda \alpha \hat{\sigma}_3 \quad (33)$$

Considering that under parity $\lambda \rightarrow -\lambda$, we can see that for a 2D system described by the Hamiltonian given by Equation (33) we have $\mathbf{h}_+ = 0$, and $\mathbf{h}_- = 2\lambda \hat{z}$, where \hat{z} is the unit vector normal to the TMD monolayer.

Using the general expressions from Equations (29)–(32) we can obtain the symmetry properties of the superconducting pair amplitudes induced by proximity in a vdW system formed by a hole-doped monolayer TMD and a generic superconducting layer:

$$S_{k,\lambda;io_n}^{even} = (\omega_n^2 + \xi_k^2 + \alpha^2) s_{k,\lambda;io_n}^{SC} - 2\lambda \alpha \xi_k \hat{z} \cdot \mathbf{d}_{k,\lambda;io_n} \quad (34)$$

$$D_{\mathbf{d},\lambda;io}^{even} = (\omega_n^2 + \xi_k^2 - \alpha^2) \mathbf{d}_{k,\lambda;io_n} + 2\alpha^2 (\hat{z} \cdot \mathbf{d}_{k,\lambda;io_n}) \hat{z} - 2\lambda \alpha \xi_k s_{k,\lambda;io_n}^{SC} \hat{z} \quad (35)$$

$$S_{k,\lambda;io_n}^{odd} = 0 \quad (36)$$

$$D_{k,\lambda;io}^{odd} = -i 2\lambda \alpha \hat{z} \times \mathbf{d}_{k,\lambda;io_n} \quad (37)$$

As described for the general case we see that the presence of SOC, proportional to α , mixes the singlet and triplet components for the even-frequency pair amplitudes. The SOC also generates an odd-frequency triplet pair amplitude proportional to the strength of the SOC in the TMD monolayer and the triplet component of the SC, Equation (37).

We now consider an effective 2D SC with Rashba SOC,^[187] which can be realized on the surface of Pb. The surface of this superconductor can be described using the Hamiltonian in Equation (20) with

$$\hat{h}_k^{SC} = \epsilon_k \hat{\sigma}_0 + \eta \hat{z} \cdot (\boldsymbol{\sigma} \times \mathbf{k}) \quad (38)$$

where ϵ_k is the spin-independent part of the electrons' dispersion and η is the strength of the Rashba SOC. The energy eigenvalues of \hat{h}_k^{SC} , $E_k = \epsilon_k \pm \eta |\mathbf{k}|$, identify the bands of the SC in the normal phase. For the order parameter, $\hat{\Delta}$, we assume, as is standard,^[187] that intraband pairing dominates and obtain the corresponding anomalous Green's function F_{SC} in the energy eigenbasis of \hat{h}_k^{SC} .

Rotating back to the spin basis in which \hat{h}_k^{SC} is expressed in Eq. (38) we obtain

$$\hat{F}_{k;i\omega_n}^{SC} = \Delta \frac{(s_{k;i\omega_n}^{SC} \hat{\sigma}_0 + \mathbf{d}_k \cdot \boldsymbol{\sigma}) i \hat{\sigma}_2}{(s_{k;i\omega_n}^{SC})^2 - |\mathbf{d}_k|^2} \quad (39)$$

where Δ is the superconducting gap, and

$$s_{k;i\omega_n}^{SC} = \Delta^2 + \omega_n^2 + \epsilon_k^2 + \eta^2 k^2 \quad (40)$$

$$\mathbf{d}_k = 2\epsilon_k \eta (-k_y, k_x, 0) \quad (41)$$

are the singlet and triplet amplitudes, respectively. Notice that the presence of Rashba SOC gives rise to a triplet component with an in-plane \mathbf{d} vector, that is, a \mathbf{d} vector that is orthogonal to the $\mathbf{h}_-(\mathbf{k})$ field due to SOC in the monolayer TMD.

From Equation (37) we see that in vdW systems composed of a TMD monolayer and an effective 2D SC with Rashba SOC an odd-frequency spin-triplet pair amplitude will be induced with strength proportional to the product of the SOC strength in the TMD and the Rashba SOC strength in the SC. In this case, the full anomalous Green's function, F^{TMD} , has the form $\hat{F}_{k,\lambda;i\omega_n}^{TMD} = A_{k,\lambda;i\omega_n}^{TMD} (F_{k,\lambda;i\omega_n}^{odd} + F_{k,\lambda;i\omega_n}^{even})$ with

$$A_{k,\lambda;i\omega_n}^{TMD} = \frac{\Delta t^2}{[(i\omega_n - \xi_k)^2 - \alpha^2]^2 [(s_{k+K_\lambda}^{SC})^2 - |\mathbf{d}_{k+K_\lambda}|^2]}$$

where $F_{k,\lambda;i\omega_n}^{even}$ and $F_{k,\lambda;i\omega_n}^{odd}$ have the same form as Equations (27) and (28) with

$$S_{k,\lambda;i\omega_n}^{even} = (\omega_n^2 + \xi_k^2 + \alpha^2) s_{k+K_\lambda}^{SC} \quad (42)$$

$$\mathbf{D}_{k,\lambda;i\omega_n}^{even} = -(\omega_n^2 + \xi_k^2 - \alpha^2) \mathbf{d}_{k+K_\lambda} - 2\lambda \alpha \xi_k s_{k+K_\lambda}^{SC} \hat{z} \quad (43)$$

$$\mathbf{D}_{k,\lambda;i\omega_n}^{odd} = i4\lambda \alpha \eta \epsilon_{k+K_\lambda} (\mathbf{k} + \mathbf{K}_\lambda) \quad (44)$$

where \mathbf{K}_λ is the momentum vector at the K (K') point for $\lambda = 1$ ($\lambda = -1$). Here, $\mathbf{D}_{k,\lambda;i\omega_n}^{odd}$ is the d-vector describing an odd-frequency spin-triplet pair amplitude. Using the above expressions, we find that this pair amplitude corresponds to a term in the anomalous Green's function of the form $F_{\uparrow\uparrow/\downarrow\downarrow}^{TMD} \sim i\omega_n \eta \alpha \epsilon_k \lambda (k_y \pm i k_x)$, where $\bar{\mathbf{k}}$ is the momentum measured from the center of the BZ.

So far we have assumed that interlayer tunneling conserves spin and is entirely spin-independent. In general, tunneling between materials with different spin eigenstates is spin-dependent. Such spin-dependence of the interlayer tunneling introduces additional mechanisms^[160–162,188,189] by which odd-frequency pairing terms can be generated in a vdW system formed by a superconducting layer and a layer with strong SOC. Such mechanisms could naturally emerge in a vdW system formed, for example, by a SC and the surface of a strong 3D TI with a “spin-active” interface, as shown schematically in Figure 9.

There are two basic mechanisms by which an interface can actively affect the spin state $|\sigma\rangle$: i) it can impart a spin-dependent phase $|\sigma\rangle_k \rightarrow e^{i\theta_{\sigma,k}} |\sigma\rangle_k$ due to the precession of the spin around a magnetic moment present at the interface; ii) the tunneling Hamiltonian can be off-diagonal in the spin basis, $\hat{t} = t_0 \hat{\sigma}_0 + \mathbf{t} \cdot \boldsymbol{\sigma}$, where \mathbf{t} is a 3-component vector, leading to spin flips. For

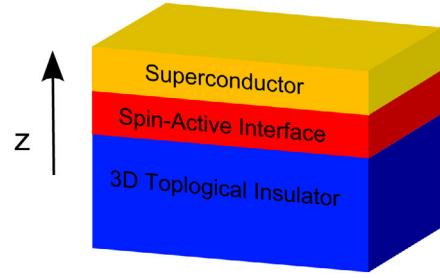


Figure 9. Schematic representation of a vdW system formed by a SC and the surface of a strong 3D TI. Adapted with permission from Phys. Rev. B 89, 165309 (2014).

case (i), when the interlayer tunneling induces a spin-dependent phase, we can see that a singlet state, $|\uparrow\rangle_k |\downarrow\rangle_{-k} - |\downarrow\rangle_k |\uparrow\rangle_{-k}$, is converted, after tunneling, to the state $e^{i\eta_k} (e^{i\zeta_k} |\uparrow\rangle_k |\downarrow\rangle_{-k} - e^{-i\zeta_k} |\downarrow\rangle_k |\uparrow\rangle_{-k})$, where $\eta_k \equiv (\theta_{\uparrow,k} + \theta_{\downarrow,k} + \theta_{\uparrow,-k} + \theta_{\downarrow,-k})/2$ and $\zeta_k \equiv (\theta_{\uparrow,k} - \theta_{\downarrow,k} - \theta_{\uparrow,-k} + \theta_{\downarrow,-k})/2$. Therefore, we see that a triplet component with amplitude proportional to $\sin \zeta_k$ emerges due to the spin-dependent phase introduced by a spin-active interface, even when the SC only has a singlet pairing.

Using the same leading-order perturbation theory discussed above we can deduce the symmetries of the proximity-induced pair amplitudes in a vdW system that possesses a spin-active interface. Here we briefly sketch how the approach leading to Equation (22) must be modified in this case, see ref. [162] for more details. To account for spin-dependent phase factors we replace the anomalous Green's function of the superconducting layer, $\hat{F}^{SC}(\mathbf{k}, \omega)$, with a rotated version:

$$\hat{F}_{\theta_k}^{SC}(\mathbf{k}, i\omega_n) = e^{i\eta_k} e^{i\frac{\delta\theta_k}{2} \sigma_3} \hat{F}^{SC}(\mathbf{k}, i\omega_n) e^{i\frac{\delta\theta_{-k}}{2} \sigma_3} \quad (45)$$

Then, we obtain the following leading-order contribution to the anomalous Green's function in the 2DEG layer:

$$\hat{F}_{k;i\omega_n}^{2D} = \hat{G}_{k;i\omega_n}^{2D} \hat{t} \hat{F}_{\theta_k}^{SC}(\mathbf{k}, i\omega_n) \hat{t}^T \left(\hat{G}_{-k;-i\omega_n}^{2D} \right)^T \quad (46)$$

From Eq. (46) we can readily deduce the symmetries of induced pair amplitudes for a variety of vdW systems by inserting the appropriate system-specific expressions for G^{2D} and F^{SC} .

In ref. [162], the pair symmetries given by Equation (46) were examined assuming a conventional spin-singlet superconducting layer. The analysis was performed for three different 2DEG layers: i) the surface of a 3D topological insulator (TI); ii) a ferromagnet with in-plane magnetization, i.e. an easy plane ferromagnet (FE); and iii) a ferromagnet with perpendicular magnetization, that is, a z-axis ferromagnet (FZ). We summarize the results in Table 1, indicating whether or not odd-frequency pairing can be realized in each of these systems for different kinds of spin-active interfaces, and its character (singlet or triplet).

From Table 1 we see that when the 2DEG layer is either an FZ or FE, odd-frequency pairing is induced for any kind of interface, while odd-frequency pairing can only be induced in the TI in the presence of spin-dependent phases. Comparing the different symmetries for the different kinds of interfaces we see that for both the FZ and FE, spin-triplet pairing is always induced. However, spin-singlet pairing can be induced in the FZ

Table 1. Conditions for the realization of odd-frequency pairing, and its spin symmetry, singlet (S) or triplet (T), for three superconductor-based vdW heterostructures, FZ-SC, FE-SC, and TI-SC, including the effect of a spin-active interface. A “—” indicates that no odd-frequency pairing is present.

Interface	FZ-SC	FE-SC	TI-SC
Not spin active	T	T	—
Spin-dep. phases	T & S	T	T
Spin flip	T	T	—
Spin-dep. phases & spin flip	T & S	T & S	T

due to spin-dependent phases, even without spin flips, while spin-singlet pairing can only be induced in the FE in the presence of both spin-dependent phases and spin flips. For the TI, the odd-frequency pairing must be spin-triplet.

We note that odd-frequency pairing has also been investigated in buckled honeycomb systems possessing proximity-induced superconductivity.^[183] In contrast to the results presented in this section, in that work the presence of the superconducting layer was accounted for by adding a spin-singlet BCS order parameter to the Kane–Mele Hamiltonian^[190,191] and computing the on-site order parameter self-consistently. For large doping, the authors found that bulk odd-frequency intersublattice pairing emerges when the sublattice symmetry is broken by, for example, an electric field perpendicular to the plane, similar to the odd-frequency interband pairing found in multiband superconductors.^[192–197] At low doping, when the low-energy states are localized at the edge of the sample, the authors performed their analysis in real space for different edge terminations, finding that odd-frequency pairing arises generically, even in the absence of an external field. In the case of the zig-zag edge termination, this was due to the asymmetry between the two sublattices at the edge.^[183] In the case of arm chair terminations, the odd-frequency pairing was due to the asymmetry between every other pair of sublattices.^[183] In both cases the odd-frequency pairing arises due to an inhomogeneity of the order parameter which naturally occurs in such finite-size systems. This phenomenon was also studied in the 2D surfaces of 3D topological insulators in the presence of an inhomogeneous superconducting order parameter,^[180] finding qualitatively similar results.

To conclude this subsection we note that the pair amplitudes given by both Equations (22) and (46) represent pairing between electrons in the same 2D layer. However, when the vdW system possesses more than one normal layer, interlayer pairing can also be important, as investigated in ref. [198]. In that work, a similar analysis to the one leading to Equations (22) was performed for a bilayer system coupled to a superconducting layer. The authors explicitly investigated the possibility of interlayer pairing. Interestingly, the authors found that, in general, because tunneling between adjacent layers dominates, an asymmetry emerges between the induced gaps on the two layers. This asymmetry leads directly to odd-frequency interlayer pairing in such vdW heterostructures,^[198] similar to phenomena studied in multiband superconductors,^[192–197] double quantum dots,^[199,200] and double nanowires.^[201,202]

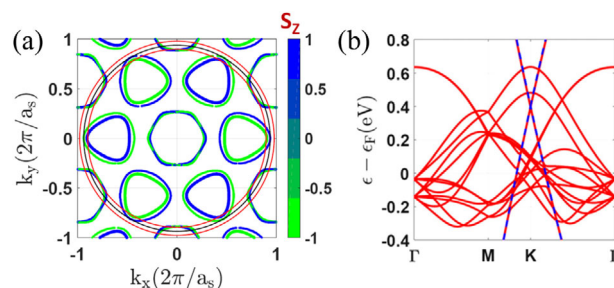


Figure 10. a) Fermi surfaces of monolayer NbSe₂. The blue (green) FSs are the NbSe₂ FSs for spin up (down) respectively, the black circle shows the position of the graphene Dirac point as θ is varied between 0 and 360°. The red circles delimit the region within which the graphene FS is confined as the twist angle is varied. b) Low energy band structure, in red, of a graphene-NbSe₂ systems obtained from ab-initio calculations including relativistic corrections for a commensurate stacking corresponding to $\theta = -65.2^\circ$. The blue lines show the low energy bands of an isolated graphene layer with doping corresponding to the charge transfer occurring when graphene is placed on NbSe₂. Adapted with permission from Phys. Rev. B. **99**, 235404 (2019)

5.2. Proximity Induced Ising Pairing

We now focus on the set of superconductor-based vdW systems in which the superconducting layer is a TMD monolayer. One of the key features of superconducting TMD monolayers is that the superconducting state is extremely robust against in-plane magnetic fields: superconductivity survives for magnetic fields much larger than the Pauli paramagnetic limit. This is due to the strong spin-splitting of the bands at the Fermi surface in metallic monolayer TMDs induced by strong SOC and a lack of inversion symmetry. These conditions favor a particular spin orientation of the Cooper pairs and the resulting superconducting pairing is termed Ising pairing.^[203,204]

The most commonly studied superconducting TMD is NbSe₂.^[203,204] The lattice structure is the same as the one shown in Figure 8a. In its monolayer form the normal state spectrum of NbSe₂ has Fermi pockets around the Γ point, and around the corners (**K** and **K'** points) of the BZ, as shown in Figure 10a. As the figure shows, the Fermi surfaces are spin-split due to SOC and broken inversion symmetry. The splitting of the Fermi surface is much stronger for the **K** and **K'** pockets than for the Γ pocket given that, at the Γ point, the **k** and $-\mathbf{k}$ states coincide. As a consequence, in the superconducting state, the pairing at the **K** and **K'** pockets is much more robust against external in-plane magnetic fields than at the Γ pocket. Such a difference is hard to detect experimentally in isolated monolayers of NbSe₂ given that even when the Zeeman term due to an in-plane magnetic field is large enough to completely suppress the superconducting gap at the Γ pocket, the superconductivity arising from the states around the **K** (**K'**) pockets survives and therefore prevents the use of transport measurements to observe the breakdown of the superconducting state at the Γ pocket.

In vdW systems formed by one monolayer of a material such as NbSe₂ and another, non-superconducting layer we can expect that the superconducting pairing induced by proximity in the normal layer will retain some of the properties of the pairing in NbSe₂ and, in particular, its Ising nature. A natural candidate

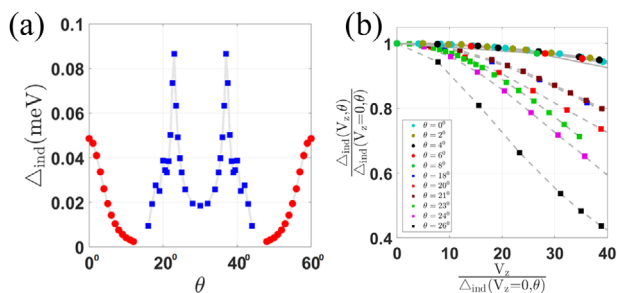


Figure 11. a) Induced superconducting gap, Δ_{ind} , into the graphene layer as a function of the twist angle. b) Δ_{ind} as a function of Zeeman field V_z . The solid lines (circles) show the results for values of θ for which graphene's FS overlaps with NbSe_2 's FS pockets around the K (K'). The dashed lines (squares) show the results for values of θ for which graphene's FS overlaps with NbSe_2 's FS pocket around the Γ point. Adapted with permission from Phys. Rev. B. **99**, 235404 (2019)

system to combine with NbSe_2 is graphene. As pointed out above, there is a large mismatch between graphene's and TMD's lattice constants and so one would expect that no significant hybridization between the graphene's and the NbSe_2 's states could take place. However, for some twist angles the Fermi pockets of NbSe_2 are large enough to overlap with graphene's Dirac points. This is displayed in Figure 10a where the green and blue lines show the spin-split Fermi surfaces of NbSe_2 , and the black circle the position of graphene's Dirac points as the twist angle θ is varied between 0 and 360° . For a range of angles, $\pm 7.2^\circ$,^[205] around 0° (and multiples of 60°) the Dirac points intersect the K (or K') Fermi pocket of NbSe_2 , and for a range of angles, $\pm 3.9^\circ$,^[205] around 21.9° (and multiples of 60°) the Dirac points intersect the Γ Fermi pocket of NbSe_2 . As a consequence, graphene can be used to probe the differences between the electronic states of the different Fermi pockets of NbSe_2 , including properties of the superconducting pairing.^[206]

Ab initio calculations^[205] show that when placed on NbSe_2 graphene becomes hole doped, Figure 10b, so that the Fermi energy in the graphene layer is ≈ 400 meV below the Dirac point. These calculations also show^[205] that the interlayer tunneling between the two systems is of the order of 20 meV and that this value, and the amount of charge transfer do not depend significantly on the twist angle. Using these values we can construct a continuum model as described in Section 2 to obtain the low-energy properties for generic values of the twist angle.

For twist angles such that the Fermi surface of graphene touches one of the Fermi pockets of NbSe_2 , superconducting pairing can be induced in the graphene layer. Figure 11a shows the value of the induced gap, Δ_{ind} , in the graphene layer as a function of the twist angle. The red circles indicate the values of Δ_{ind} for the cases when the graphene FS touches the K (K') Fermi pocket of NbSe_2 . The blue squares denote the cases when the graphene FS touches the NbSe_2 Fermi pocket around the Γ point. These results show that in superconductor-based vdW systems such as NbSe_2 -graphene heterostructures, the size of the gap induced by proximity can be strongly tuned by varying the twist angle.

Figure 11b shows how the proximity-induced superconducting gap in the graphene layer depends on the strength of a Zeeman term, V_z , due to the presence of an in-plane magnetic field,

for different values of the twist angle. The solid lines with circles show the results for values of θ such that the low energy states in graphene hybridize with the low energy states close to the K (K') point in NbSe_2 . The dashed lines with squares show the results for the cases where the graphene FS touches the NbSe_2 Fermi pocket at the Γ point. We see that in the first case the induced superconducting gap is much more robust against the presence of an in-plane field than in the second case. This is a consequence of the fact that, for the first case, the graphene is effectively probing the superconducting gap of NbSe_2 at the K (K') where the spin-splitting due to the SOC is much stronger than for the pocket around the Γ pocket, and therefore the Ising nature of the pairing is much more pronounced.

The results of Figure 11b show that in vdW systems like graphene- NbSe_2 , the Ising character of the induced superconducting pairing can be tuned via the twist angle. In addition, they show that in these types of structures graphene can be used to probe the relative strength of the gaps on different parts of the FS of the substrate, and the robustness of these gaps to external magnetic fields.

6. Conclusions

In this article we have reviewed recent work on heterogenous van der Waals systems in which one of the components has strong spin-orbit coupling. The field of van der Waals systems is now very large and so we have restricted the discussion to a few exemplary vdW systems.

We first presented the general effective model to obtain the low energy electronic spectrum for a generic stacking configuration. The model relies on parameters that must be obtained via ab initio calculations, or, when possible, directly from experimental measurements. We then discussed, in detail, the case of a van der Waals system formed by coupling a single layer of graphene to the surface of a three dimensional strong topological insulator. We discussed how the hybridization between the states in these two systems strongly enhances the spin-orbit coupling of the graphene layer. We then considered the electronic transport of graphene-TI bilayers and showed how the enhancement of the spin-orbit coupling in graphene, and the additional screening of charge impurities by the graphene layer, can lead to a considerable amplification of spin-dependent effects, such as the Edelstein effect. We briefly discussed the case of heterostructures formed by graphene and semiconducting transition metal dichalcogenides.

In the second part of the work we discussed the case of heterogenous vdW systems in which one of the components is superconducting. Given the scope of this special issue, particular focus was placed on systems in which odd-frequency pairing can be realized. We first presented a general analysis allowing the identification of conditions for realizing odd-frequency pairing based on a combination of proximity-induced superconductivity and spin-orbit coupling in superconductor-based vdW systems. Based on this general treatment, we observed that vdW systems with spin-orbit coupling are ideal systems for realizing odd-frequency pair correlations. A distinct advantage over bulk superconductors with a similar degree of spin-orbit coupling is that the direction of the field describing the spin-orbit coupling and

that of the \mathbf{d}_k vector describing the spin configuration of a triplet superconductor can be completely different since they belong to different layers in the vdW system. After this general discussion, we examined a concrete example in which this condition can be realized: a vdW system formed by a monolayer transition metal dichalcogenide and a 2D superconductor with Rashba spin-orbit coupling. We then discussed the case of vdW systems in which the interface between the superconducting layer and the normal layer causes the interlayer tunneling to be spin-dependent. We reviewed the conditions under which such a “spin-active” interface can lead to the formation of odd-frequency superconducting pairing. Finally, we discussed the case in which the superconducting layer exhibits Ising superconductivity, as in monolayer NbSe₂. In particular, we saw that in graphene-NbSe₂vdW systems, the size of the superconducting gap and its robustness against in-plane magnetic fields, strongly depend on the relative twist angle between the layers.

Our brief survey of the field shows that van der Waals heterostructures in which spin-orbit coupling is present constitute a very interesting class of systems, both from a fundamental point of view, and for technological applications. The freedom in the selection of the layers forming the heterostructure, combined with the ability to control the stacking configuration, mean that the number of vdW systems with spin-orbit that can be realized, and that have not been studied yet is very large. This presents the opportunity to realize vdW systems with spin-orbit coupling exhibiting novel spin dependent transport properties or in which known spintronics effects can be optimized and deployed effectively in technological applications. A class of vdW systems with spin-orbit coupling that would be very interesting to study, and that is still largely unexplored, is the one in which the presence of spin-orbit is coupled to strong electron–electron correlations. Such coupling could perhaps be realized in vdW heterostructures combining twisted bilayer graphene and layers with strong spin-orbit coupling. The study of the response to several external probes, in particular time-dependent probes, of the type of vdW systems described in this survey is still largely unexplored. Another interesting direction is the study of vdW systems with spin-orbit coupling in which one of the constituents is a nanostructure, such as heterostructures formed by graphene nanoribbons and substrates with strong spin-orbit coupling. These structures could allow the realization of nano-devices with tunable spin-orbit coupling.

One of the challenges to understand the physics of vdW systems, and to use them in applications, is the correct characterization of the effects of disorder. For some vdW systems the dominant source of disorder is still unknown. In some vdW structures the twist angle is not spatially homogenous and the effect of the randomness of the twist angle on the transport properties is not known yet. Also still unknown is why in graphene-based structures the experimentally measured spin-relaxation time is orders of magnitude smaller than the theoretical predictions. In the case of superconductor-based vdW systems, a major driver in the field has been the engineering of exotic superconducting states, in particular those which possess unconventional symmetries like odd-frequency pairing. Two major barriers to understanding these exotic states are the scarcity of unambiguous experimental signatures, and the difficulty of realizing systems in which the odd-frequency pairing dominates the even-frequency. While these barriers have been overcome in particular experi-

mental setups, as discussed in Section 5.1, a general solution to the problem is still lacking.

We emphasize that one of the most interesting features of van der Waals systems is that the choice of layers is, to a large extent, not constrained by chemistry. On top of the flexibility in the choice of constituent layers, recent experimental developments demonstrating that the relative twist angle between layers can be controlled within a fraction of degree allow for an incredible amount of tunability of the interlayer coupling. As we have seen in our discussion of just a limited sample of possible van der Waals systems with spin-orbit coupling, the ability to combine layers with different properties can be used to realize and control exotic superconducting states and engineer systems with strong spin-dependent transport effects. By continuing to study the myriad combinations of the growing number of 2D crystals, we expect many more novel and surprising electronic properties will be discovered in van der Waals structures.

Acknowledgements

It is a pleasure to thank the many collaborators with whom the authors have had the opportunity to work in the past few years on the topics discussed in this article: D. S. L. Abergel, E. Y. Andrei, D. M. Badiane, A. V. Balatsky, A. M. Black-Schaffer, J. Cayao, Y. Gaucher, Y. S. Gani, R. M. Geilhufe, Y. Kedem, D. Kuzmanovski, E. Langmann, Chih-Pin Lu, T. Löthman, M. Mashkooi, F. Parhizgar M. Rodriguez-Vega, G. Schwiete, J. Sinova, H. Steinberg, and Junhua Zhang.

The work of E.R. has been supported by NSF CAREER Grant No. DMR-1350663, ONR Grants No. ONR-N00014-13-1-0321, No. ONR-N00014-16-1-3158, ARO Grants No. W911NF-16-1-0387, No. W911NF-18-1-0290, BSF Grant No 2016320, and by the computing facilities at William & Mary which were provided by contributions from the NSF, the Commonwealth of Virginia Equipment Trust Fund, and ONR. E.R. also thanks the Aspen Center for Physics, which is supported by National Science Foundation grant PHY-1607611, where part of this work was performed.

Conflict of Interest

The authors declare no conflict of interest.

Keywords

graphene, odd-frequency superconductivity, topological materials, twisted bilayers, van der Waals systems

Received: August 2, 2019

Revised: October 16, 2019

Published online: December 29, 2019

- [1] A. K. Geim, K. S. Novoselov, *Nat. Mater.* **2007**, *6*, 183.
- [2] A. K. Geim, I. V. Grigorieva, *Nature* **2013**, *499*, 419.
- [3] Y. Liu, N. O. Weiss, X. Duan, H. C. Cheng, Y. Huang, X. Duan, *Nat. Rev. Mat.* **2016**, *1*, 16042.
- [4] K. S. Novoselov, A. Mishchenko, A. Carvalho, A. H. Castro Neto, *Science* **2016**, *353*, aac9439.
- [5] K. S. Novoselov, A. K. Geim, S. V. Morozov, D. Jiang, Y. Zhang, S. V. Dubonos, I. V. Grigorieva, A. A. Firsov, *Science* **2004**, *306*, 666.

- [6] A. H. C. Neto, F. Guinea, N. M. R. Peres, K. S. Novoselov, A. K. Geim, *Rev. Mod. Phys.* **2009**, *81*, 109.
- [7] S. Das Sarma, S. Adam, E. H. Hwang, E. Rossi, *Rev. Mod. Phys.* **2011**, *83*, 407.
- [8] Y. Cao, V. Fatemi, S. Fang, K. Watanabe, T. Taniguchi, E. Kaxiras, P. Jarillo-Herrero, *Nature* **2018**, *556*, 43.
- [9] Y. Cao, V. Fatemi, A. Demir, S. Fang, S. L. Tomarken, J. Y. Luo, J. D. Sanchez-Yamagishi, K. Watanabe, T. Taniguchi, E. Kaxiras, R. C. Ashoori, P. Jarillo-Herrero, *Nature* **2018**, *556*, 80.
- [10] M. Yankowitz, S. Chen, H. Polshyn, Y. Zhang, K. Watanabe, T. Taniguchi, D. Graf, A. F. Young, C. R. Dean, *Science* **2019**, *363*, 1059.
- [11] H. Zhang, C. Liu, X. Qi, X. Dai, Z. Fang, S. Zhang, *Nat. Phys.* **2009**, *5*, 438.
- [12] M. Hasan, C. Kane, *Rev. Mod. Phys.* **2010**, *82*, 3045.
- [13] X. L. Qi, S. C. Zhang, *Rev. Mod. Phys.* **2011**, *83*, 1057.
- [14] J. Zhang, C. Triola, E. Rossi, *Phys. Rev. Lett.* **2014**, *112*, 096802.
- [15] D. Khokhriakov, A. W. Cummings, K. Song, M. Vila, B. Karpiak, A. Dankert, S. Roche, S. P. Dash, *Sci. Adv.* **2018**, *4*, eaat9349.
- [16] C. Triola, D. M. Badiane, A. V. Balatsky, E. Rossi, *Phys. Rev. Lett.* **2016**, *116*, 257001.
- [17] K. S. Burch, D. Mandrus, J. G. Park, *Nature* **2018**, *563*, 47.
- [18] Ø. Johansen, V. Risinggård, A. Sudbø, J. Linder, A. Brataas, *Phys. Rev. Lett.* **2019**, *122*, 217203.
- [19] C. Gong, X. Zhang, *Science* **2019**, *363*, eaav4450.
- [20] J. U. Lee, S. Lee, J. H. Ryoo, S. Kang, T. Y. Kim, P. Kim, C. H. Park, J. G. Park, H. Cheong, *Nano Lett.* **2016**, *16*, 7433.
- [21] C. Gong, L. Li, Z. Li, H. Ji, A. Stern, Y. Xia, T. Cao, W. Bao, C. Wang, Y. Wang, Z. Q. Qiu, R. J. Cava, S. G. Louie, J. Xia, X. Zhang, *Nature* **2017**, *546*, 265.
- [22] B. Huang, G. Clark, E. Navarro-Moratalla, D. R. Klein, R. Cheng, K. L. Seyler, D. Zhong, E. Schmidgall, M. A. McGuire, D. H. Cobden, W. Yao, D. Xiao, P. Jarillo-Herrero, X. Xu, *Nature* **2017**, *546*, 270.
- [23] D. R. Klein, D. MacNeill, J. L. Lado, D. Soriano, E. Navarro-Moratalla, K. Watanabe, T. Taniguchi, S. Manni, P. Canfield, J. Fernández-Rossier, P. Jarillo-Herrero, *Science* **2018**, *360*, 1218.
- [24] M. Bonilla, S. Kolekar, Y. Ma, H. C. Diaz, V. Kalappattil, R. Das, T. Eggers, H. R. Gutierrez, M. H. Phan, M. Batzill, *Nat. Nanotechnol.* **2018**, *13*, 289.
- [25] D. J. O'Hara, T. Zhu, A. H. Trout, A. S. Ahmed, Y. K. Luo, C. H. Lee, M. R. Brenner, S. Rajan, J. A. Gupta, D. W. McComb, R. K. Kawakami, *Nano Lett.* **2018**, *18*, 3125.
- [26] Z. Fei, B. Huang, P. Malinowski, W. Wang, T. Song, J. Sanchez, W. Yao, D. Xiao, X. Zhu, A. F. May, W. Wu, D. H. Cobden, J. H. Chu, X. Xu, *Nat. Mater.* **2018**, *17*, 778.
- [27] Y. Deng, Y. Yu, Y. Song, J. Zhang, N. Z. Wang, Z. Sun, Y. Yi, Y. Z. Wu, S. Wu, J. Zhu, J. Wang, X. H. Chen, Y. Zhang, *Nature* **2018**, *563*, 94.
- [28] J. Hauser, *Phys. Rev.* **1969**, *187*, 580.
- [29] P. Lazić, K. Belashchenko, I. Žutić, *Phys. Rev. B* **2016**, *93*, 241401.
- [30] X. Liang, L. Deng, F. Huang, T. Tang, C. Wang, Y. Zhu, J. Qin, Y. Zhang, B. Peng, L. Bi, *Nanoscale* **2017**, *9*, 9502.
- [31] N. Cortés, O. Ávalos-Ovando, L. Rosales, P. A. Orellana, S. E. Ulloa, *Phys. Rev. Lett.* **2019**, *122*, 086401.
- [32] P. Vogt, P. De Padova, C. Quaresima, J. Avila, E. Frantzeskakis, M. C. Asensio, A. Resta, B. Ealet, G. Le Lay, *Phys. Rev. Lett.* **2012**, *108*, 155501.
- [33] C. C. Liu, W. Feng, Y. Yao, *Phys. Rev. Lett.* **2011**, *107*, 076802.
- [34] M. Dávila, L. Xian, S. Cahangirov, A. Rubio, G. Le Lay, *New J. Phys.* **2014**, *16*, 095002.
- [35] F. f. Zhu, W. j. Chen, Y. Xu, C. L. Gao, D. d. Guan, C. h. Liu, D. Qian, S. C. Zhang, J. f. Jia, *Nat. Mater.* **2015**, *14*, 1020.
- [36] Y. S. Gani, D. S. L. Abergel, E. Rossi, *Phys. Rev. B* **2018**, *98*, 205415.
- [37] K. Kośmider, J. Fernández-Rossier, *Phys. Rev. B* **2013**, *87*, 075451.
- [38] Y. Wang, Z. Wang, W. Yao, G. B. Liu, H. Yu, *Phys. Rev. B* **2017**, *95*, 115429.
- [39] Y. Li, Q. Cui, F. Ceballos, S. D. Lane, Z. Qi, H. Zhao, *Nano Lett.* **2017**, *17*, 6661.
- [40] F. Wu, T. Lovorn, E. Tutuc, I. Martin, A. MacDonald, *Phys. Rev. Lett.* **2019**, *122*, 086402.
- [41] H. Yu, M. Chen, W. Yao, *arXiv preprint 1906.05499*, **2019**.
- [42] S. Carr, S. Fang, P. Jarillo-Herrero, E. Kaxiras, *Phys. Rev. B* **2018**, *98*, 085144.
- [43] Y. Jiang, X. Lai, K. Watanabe, T. Taniguchi, K. Haule, J. Mao, E. Y. Andrei, *Nature* **2019**, *573*, 91.
- [44] B. Hunt, J. D. Sanchez-Yamagishi, A. F. Young, M. Yankowitz, B. J. LeRoy, K. Watanabe, T. Taniguchi, P. Moon, M. Koshino, P. Jarillo-Herrero, R. C. Ashoori, *Science* **2013**, *340*, 1427.
- [45] J. Jung, A. M. Dasilva, A. H. Macdonald, S. Adam, *Nat. Commun.* **2015**, *6*, 6308.
- [46] M. Yankowitz, K. Watanabe, T. Taniguchi, P. San-Jose, B. J. LeRoy, *Nat. Commun.* **2016**, *7*, 13168.
- [47] J. Lopes dos Santos, N. Peres, A. Castro Neto, *Phys. Rev. Lett.* **2007**, *99*, 256802.
- [48] E. S. Morell, J. D. Correa, P. Vargas, M. Pacheco, Z. Barticevic, *Phys. Rev. B* **2010**, *82*, 121407.
- [49] R. Bistritzer, A. H. MacDonald, *Proc. Natl. Acad. Sci. USA* **2011**, *108*, 12233.
- [50] Y. S. Gani, H. Steinberg, E. Rossi, *Proc. Natl. Acad. Sci. USA* **2019**, *99*, 235404.
- [51] H. Steinberg, L. A. Orona, V. Fatemi, J. D. Sanchez-Yamagishi, K. Watanabe, T. Taniguchi, P. Jarillo-Herrero, *Phys. Rev. B* **2015**, *92*, 241409.
- [52] G. Bian, T. F. Chung, C. Chen, C. Liu, T. R. Chang, T. Wu, I. Belopolski, H. Zheng, S. Y. Xu, D. S. Sanchez, N. Alidoust, J. Pierce, B. Quilliams, P. P. Barletta, S. Lorcy, J. Avila, G. Chang, H. Lin, H. T. Jeng, M. C. Asensio, Y. P. Chen, M. Z. Hasan, *2D Mater.* **2016**, *3*, 021009.
- [53] K. H. Jin, S. H. Jhi, *Phys. Rev. B* **2013**, *87*, 075442.
- [54] K. Song, D. Soriano, A. W. Cummings, R. Robles, P. Ordejón, S. Roche, *Nano Lett.* **2018**, *18*, 2033.
- [55] W. Cao, R. X. Zhang, P. Tang, G. Yang, J. Sofo, W. Duan, C. X. Liu, *2D Mater.* **2016**, *3*, 034006.
- [56] H. J. Zhang, C. X. Liu, X. L. Qi, X. Dai, Z. Fang, S. C. Zhang, *Nature Phys.* **2009**, *5*, 438.
- [57] C. X. Liu, X. L. Qi, H. Zhang, X. Dai, Z. Fang, S. C. Zhang, *Phys. Rev. B* **2010**, *82*, 045122.
- [58] Z. Ren, A. A. Taskin, S. Sasaki, K. Segawa, Y. Ando, *Phys. Rev. B* **2010**, *82*, 241306.
- [59] T. Arakane, T. Sato, S. Souma, K. Kosaka, K. Nakayama, M. Komatsu, T. Takahashi, Z. Ren, K. Segawa, Y. Ando, *Nat. Commun.* **2012**, *3*, 636.
- [60] B. Xia, P. Ren, A. Sulaev, P. Liu, S. Q. Shen, L. Wang, *Phys. Rev. B* **2013**, *87*, 085442.
- [61] K. Segawa, Z. Ren, S. Sasaki, T. Tsuda, S. Kuwabata, Y. Ando, *Phys. Rev. B* **2012**, *86*, 075306.
- [62] Y. Xu, I. Miotkowski, C. Liu, J. Tian, H. Nam, N. Alidoust, J. Hu, C. K. Shih, M. Z. Hasan, Y. P. Chen, *Nat. Phys.* **2014**, *10*, 956.
- [63] C. Durand, X. G. Zhang, S. M. Hus, C. Ma, M. A. McGuire, Y. Xu, H. Cao, I. Miotkowski, Y. P. Chen, A. P. Li, *Nano Lett.* **2016**, *16*, 2213.
- [64] Y. Xu, I. Miotkowski, Y. P. Chen, *Nat. Commun.* **2016**, *7*, 11434.
- [65] K. Nomura, A. H. MacDonald, *Phys. Rev. Lett.* **2006**, *96*, 256602.
- [66] S. Adam, E. H. Hwang, V. M. Galitski, S. Das Sarma, *Proc. Natl. Acad. Sci. USA* **2007**, *104*, 18392.
- [67] E. Rossi, S. Adam, S. D. Sarma, *Phys. Rev. B* **2009**, *79*, 245423.
- [68] S. D. Sarma, E. H. Hwang, E. Rossi, *Phys. Rev. B* **2010**, *81*, 161407(R).
- [69] Q. Li, E. H. Hwang, E. Rossi, S. Das Sarma, *Phys. Rev. Lett.* **2011**, *107*, 156601.
- [70] E. Rossi, S. Das Sarma, *Phys. Rev. Lett.* **2011**, *107*, 155502.
- [71] E. Rossi, J. H. Bardarson, M. S. Fuhrer, S. Das Sarma, *Phys. Rev. Lett.* **2012**, *109*, 096801.

- [72] Q. Li, E. H. Hwang, E. Rossi, *Solid State Commun.* **2012**, *152*, 1390.
- [73] A. A. Burkov, A. S. Núñez, A. H. MacDonald, *Phys. Rev. B* **2004**, *70*, 155308.
- [74] A. A. Burkov, D. G. Hawthorn, *Phys. Rev. Lett.* **2010**, *105*, 066802.
- [75] J. Sinova, S. O. Valenzuela, J. Wunderlich, C. H. Back, T. Jungwirth, *Rev. Mod. Phys.* **2015**, *87*, 1213.
- [76] E. H. Hwang, S. Das Sarma, *Phys. Rev. B* **2007**, *75*, 205418.
- [77] B. I. Shklovskii, *Phys. Rev. B* **2007**, *76*, 233411.
- [78] G. Borghi, M. Polini, R. Asgari, A. H. MacDonald, *Phys. Rev. B* **2009**, *80*, 241402.
- [79] D. S. L. Abergel, E. Rossi, S. Das Sarma, *Phys. Rev. B* **2012**, *86*, 155447.
- [80] C. Triola, E. Rossi, *Phys. Rev. B* **2012**, *86*, 161408.
- [81] C. P. Lu, M. Rodriguez-Vega, G. Li, A. Luican-Mayer, K. Watanabe, T. Taniguchi, E. Rossi, E. Y. Andrei, *Proc. Natl. Acad. Sci. USA* **2016**, *113*, 6623.
- [82] M. Rodriguez-Vega, G. Schwiete, J. Sinova, E. Rossi, *Phys. Rev. B* **2017**, *96*, 235419.
- [83] E. Rossi, S. Das Sarma, *Phys. Rev. Lett.* **2008**, *101*, 166803.
- [84] D. Culcer, E. H. Hwang, T. D. Stanescu, S. Das Sarma, *Phys. Rev. B* **2010**, *82*, 155457.
- [85] Q. Li, E. Rossi, S. Das Sarma, *Phys. Rev. B* **2012**, *86*, 235443.
- [86] S. Adam, E. H. Hwang, S. D. Sarma, *Phys. Rev. B* **2012**, *85*, 235413.
- [87] B. Skinner, T. R. Chen, B. I. Shklovskii, *Phys. Rev. Lett.* **2012**, *109*, 176801.
- [88] B. Skinner, B. I. Shklovskii, *Phys. Rev. B* **2013**, *87*, 075454.
- [89] N. P. Butch, K. Kirshenbaum, P. Syers, A. B. Sushkov, G. S. Jenkins, H. D. Drew, J. Paglione, *Phys. Rev. B* **2010**, *81*, 241301.
- [90] H. Beidenkopf, P. Roushan, J. Seo, L. Gorman, I. Drozdov, Y. S. Hor, R. J. Cava, A. Yazdani, *Nat. Phys.* **2011**, *7*, 939.
- [91] D. Kim, S. Cho, N. P. Butch, P. Syers, K. Kirshenbaum, S. Adam, J. Paglione, M. S. Fuhrer, *Nat. Phys.* **2012**, *8*, 458.
- [92] M. Rodriguez-Vega, J. Fischer, S. Das Sarma, E. Rossi, *Phys. Rev. B* **2014**, *90*, 035406.
- [93] M. I. Dyakonov, V. I. Perel, *Phys. Lett. A* **1971**, *A 35*, 459.
- [94] V. M. Edelstein, *Solid State Comm.* **1990**, *73*, 233.
- [95] I. Garate, M. Franz, *Phys. Rev. Lett.* **2010**, *104*, 146802.
- [96] T. Yokoyama, Y. Tanaka, N. Nagaosa, *Phys. Rev. B* **2010**, *81*, 121401.
- [97] A. Sakai, H. Kohno, *Phys. Rev. B* **2014**, *89*, 165307.
- [98] M. H. Fischer, A. Vaezi, A. Manchon, E. A. Kim, *Phys. Rev. B* **2016**, *93*, 125303.
- [99] A. R. Mellnik, J. S. Lee, A. Richardella, J. L. Grab, P. J. Mintun, M. H. Fischer, A. Vaezi, A. Manchon, E. A. Kim, N. Samarth, D. C. Ralph, *Nature* **2014**, *511*, 449.
- [100] Y. Fan, X. Kou, P. Upadhyaya, Q. Shao, L. Pan, M. Lang, X. Che, J. Tang, M. Montazeri, K. Murata, L.-T. Chang, M. Akyol, G. Yu, T. Nie, K. L. Wong, J. Liu, Y. Wang, Y. Tserkovnyak, K. L. Wang, *Nat. Nanotechnol.* **2016**, *11*, 352.
- [101] M. Rodriguez-Vega, G. Schwiete, E. Rossi, *Phys. Rev. Res.* **2019**, *1*, 033085.
- [102] D. Xiao, G. B. Liu, W. Feng, X. Xu, W. Yao, *Phys. Rev. Lett.* **2012**, *108*, 196802.
- [103] A. Ramasubramanian, *Phys. Rev. B* **2012**, *86*, 115409.
- [104] Q. H. Wang, K. Kalantar-Zadeh, A. Kis, J. N. Coleman, M. S. Strano, *Nat. Nanotechnol.* **2012**, *7*, 699.
- [105] X. Xu, W. Yao, D. Xiao, T. F. Heinz, *Nat. Phys.* **2014**, *10*, 343.
- [106] D. W. Latzke, W. Zhang, A. Suslu, T. R. Chang, H. Lin, H. T. Jeng, S. Tongay, J. Wu, A. Bansil, A. Lanzara, *Phys. Rev. B* **2015**, *91*, 235202.
- [107] D. Xiao, G. B. Liu, W. Feng, X. Xu, W. Yao, *Phys. Rev. Lett.* **2012**, *108*, 196802.
- [108] M. Gmitra, S. Konschuh, C. Ertler, C. Ambrosch-Draxl, J. Fabian, *Phys. Rev. B* **2009**, *80*, 235431.
- [109] M. Gmitra, J. Fabian, *Phys. Rev. B* **2015**, *92*, 155403.
- [110] M. Gmitra, D. Kochan, P. Högl, J. Fabian, *Phys. Rev. B* **2016**, *93*, 155104.
- [111] M. Gmitra, J. Fabian, *Phys. Rev. Lett.* **2017**, *119*, 146401.
- [112] A. M. Alsharari, M. M. Asmar, S. E. Ulloa, *Phys. Rev. B* **2016**, *94*, 241106.
- [113] A. M. Alsharari, M. M. Asmar, S. E. Ulloa, *Phys. Rev. B* **2018**, *98*, 195129.
- [114] A. M. Alsharari, M. M. Asmar, S. E. Ulloa, *Phys. Rev. B* **2018**, *97*, 241104.
- [115] Z. Wang, D. Ki, H. Chen, H. Berger, A. H. MacDonald, A. F. Morpurgo, *Nat. Commun.* **2015**, *6*, 8339.
- [116] Z. Wang, D.-K. Ki, J. Y. Khoo, D. Mauro, H. Berger, L. S. Levitov, A. F. Morpurgo, *Phys. Rev. X* **2016**, *6*, 041020.
- [117] B. Yang, M. F. Tu, J. Kim, Y. Wu, H. Wang, J. Alicea, R. Wu, M. Bockrath, J. Shi, *2D Mater.* **2016**, *3*, 031012.
- [118] B. Yang, M. Lohmann, D. Barroso, I. Liao, Z. Lin, Y. Liu, L. Bartels, K. Watanabe, T. Taniguchi, J. Shi, *Phys. Rev. B* **2017**, *96*, 041409.
- [119] T. Völkl, T. Rockinger, M. Drienovsky, K. Watanabe, T. Taniguchi, D. Weiss, J. Eroms, *Phys. Rev. B* **2017**, *96*, 125405.
- [120] T. Wakamura, F. Reale, P. Palczynski, S. Gueron, C. Mattevi, H. Bouchiat, *Phys. Rev. Lett.* **2018**, *120*, 106802.
- [121] S. Zihlmann, A. W. Cummings, J. H. Garcia, M. Kedves, K. Watanabe, T. Taniguchi, C. Schönenberger, P. Makk, *Phys. Rev. B* **2018**, *97*, 075434.
- [122] A. Avsar, J. Y. Tan, T. Taychatanapat, J. Balakrishnan, G. Koon, Y. Yeo, J. Lahiri, A. Carvalho, A. S. Rodin, E. O'Farrell, G. Eda, A. H. Castro Neto, B. Özyilmaz, *Nat. Commun.* **2014**, *5*, 4875.
- [123] A. Dankert, S. P. Dash, *Nat. Commun.* **2017**, *8*, 16093.
- [124] T. S. Ghiasi, J. Ingla-Aynés, A. A. Kaverzin, B. J. van Wees, *Nano Lett.* **2017**, *17*, 7528.
- [125] S. Omar, B. J. van Wees, *Phys. Rev. B* **2018**, *97*, 045414.
- [126] L. A. Benítez, J. F. Sierra, W. Saverio Torres, A. Arrighi, F. Bonell, M. V. Costache, S. O. Valenzuela, *Nat. Phys.* **2018**, *14*, 303.
- [127] Y. Li, M. Koshino, *Phys. Rev. B* **2019**, *99*, 075438.
- [128] A. David, P. Rakyta, A. Kormányos, G. Burkard, *Phys. Rev. B* **2019**, *100*, 085412.
- [129] M. Offidani, M. Milletari, R. Raimondi, A. Ferreira, *Phys. Rev. Lett.* **2017**, *119*, 246801.
- [130] J. H. Garcia, A. W. Cummings, S. Roche, *Nano Lett.* **2017**, *17*, 5078.
- [131] W. Yan, O. Txoperena, R. Llopis, H. Dery, L. E. Hueso, F. Casanova, *Nat. Commun.* **2016**, *7*, 13372.
- [132] C. K. Safeer, J. Ingla-Aynés, F. Herling, J. H. Garcia, M. Vila, N. Ontoso, M. R. Calvo, S. Roche, L. E. Hueso, F. Casanova, *Nano Lett.* **2019**, *19*, 1074.
- [133] T. S. Ghiasi, A. A. Kaverzin, P. J. Blah, B. J. van Wees, *Nano Lett.* **2019**, *19*, 5959.
- [134] L. A. Benitez, W. S. Torres, J. F. Sierra, M. Timmermans, J. H. Garcia, S. Roche, M. V. Costache, S. O. Valenzuela, *arXiv preprint arXiv:1908.07868*, **2019**.
- [135] A. M. Hoque, D. Khokhriakov, B. Karpiak, S. P. Dash, *arXiv preprint arXiv:1908.09367*, **2019**.
- [136] L. Li, J. Zhang, G. Myeong, W. Shin, H. Lim, B. Kim, S. Kim, T. Jin, B. Kim, C. Kim, J. Lischner, A. Ferreira, S. Cho, *arXiv preprint arXiv:1906.10702*, **2019**.
- [137] J. O. Island, X. Cui, C. Lewandowski, J. Y. Khoo, E. M. Spanton, H. Zhou, D. Rhodes, J. C. Hone, T. Taniguchi, K. Watanabe, L. S. Levitov, M. P. Zaletel, A. F. Young, *Nature* **2019**, *571*, 85.
- [138] L. Fu, C. L. Kane, *Phys. Rev. Lett.* **2008**, *100*, 096407.
- [139] J. D. Sau, R. M. Lutchyn, S. Tewari, S. D. Sarma, *Phys. Rev. Lett.* **2010**, *104*, 040502.
- [140] R. M. Lutchyn, J. D. Sau, S. D. Sarma, *Phys. Rev. Lett.* **2010**, *105*, 077001.
- [141] Y. Oreg, G. Refael, F. von Oppen, *Phys. Rev. Lett.* **2010**, *105*, 177002.

- [142] A. E. Antipov, A. Bargerbos, G. W. Winkler, B. Bauer, E. Rossi, R. M. Lutchyn, *Phys. Rev. X* **2018**, 8, 031041.
- [143] F. S. Bergeret, A. F. Volkov, K. B. Efetov, *Rev. Mod. Phys.* **2005**, 77, 1321.
- [144] J. Linder, A. V. Balatsky, *arXiv:1709.03986*, **2017**.
- [145] V. L. Berezhinskiĭ, *Sov. J. Exper. Theor. Phys. Lett.* **1974**, 20, 287.
- [146] T. R. Kirkpatrick, D. Belitz, *Phys. Rev. Lett.* **1991** 66, 1533.
- [147] D. Belitz, T. R. Kirkpatrick, *Phys. Rev. B* **1992**, 46, 8393.
- [148] A. Balatsky, E. Abrahams, *Phys. Rev. B* **1992**, 45, 13125.
- [149] P. Coleman, E. Miranda, A. Tsvetik, *Phys. Rev. Lett.* **1993**, 70, 2960.
- [150] P. Coleman, E. Miranda, A. Tsvetik, *Phys. Rev. Lett.* **1995**, 74, 1653.
- [151] D. Belitz, T. R. Kirkpatrick, *Phys. Rev. B* **1999**, 60, 3485.
- [152] E. Abrahams, A. Balatsky, J. Schrieffer, P. B. Allen, *Phys. Rev. B* **1993**, 47, 513.
- [153] P. Coleman, E. Miranda, A. Tsvetik, *Phys. Rev. B* **1994**, 49, 8955.
- [154] O. Dolgov, V. Losyakov, *Phys. Lett. A* **1994**, 190, 189.
- [155] R. Heid, *Z. Phys. B: Condens. Matter* **1995**, 99, 15.
- [156] F. Bergeret, A. Volkov, K. Efetov, *Phys. Rev. Lett.* **2001**, 86, 4096.
- [157] K. Halterman, P. H. Barsic, O. T. Valls, *Phys. Rev. Lett.* **2007**, 99, 127002.
- [158] T. Yokoyama, Y. Tanaka, A. A. Golubov, *Phys. Rev. B* **2007**, 75, 134510.
- [159] M. Houzet, *Phys. Rev. Lett.* **2008**, 101, 057009.
- [160] M. Eschrig, T. Löfwander, *Nat. Phys.* **2008**, 4, 138.
- [161] J. Linder, T. Yokoyama, A. Sudbø, *Phys. Rev. B* **2008**, 77, 174514.
- [162] C. Triola, E. Rossi, A. V. Balatsky, *Phys. Rev. B* **2014**, 89, 165309.
- [163] F. Crépin, P. Burset, B. Trauzettel, *Phys. Rev. B* **2015**, 92, 100507.
- [164] V. Petrashov, V. Antonov, S. Maksimov, R. S. Shaikhdarov, *JETP Lett.* **1994**, 59, 551.
- [165] M. Giroud, H. Courtois, K. Hasselbach, D. Maily, B. Pannetier, *Phys. Rev. B* **1998**, 58, R11872.
- [166] V. Petrashov, I. Sosnin, I. Cox, A. Parsons, C. Troadec, *Phys. Rev. Lett.* **1999**, 83, 3281.
- [167] J. Aumentado, V. Chandrasekhar, *Phys. Rev. B* **2001**, 64, 054505.
- [168] J. Zhu, I. N. Krivorotov, K. Halterman, O. T. Valls, *Phys. Rev. Lett.* **2010**, 105, 207002.
- [169] A. Di Bernardo, S. Diesch, Y. Gu, J. Linder, G. Divitini, C. Ducati, E. Scheer, M. G. Blamire, J. W. Robinson, *Nat. Commun.* **2015**, 6, 8053.
- [170] A. Di Bernardo, Z. Salman, X. L. Wang, M. Amado, M. Egilmez, M. G. Flokstra, A. Suter, S. L. Lee, J. H. Zhao, T. Prokscha, E. Morenzoni, M. G. Blamire, J. Linder, J. W. A. Robinson, *Phys. Rev. X* **2015**, 5, 041021.
- [171] Y. Tanaka, A. A. Golubov, *Phys. Rev. Lett.* **2007**, 98, 037003.
- [172] Y. Tanaka, Y. Tanuma, A. Golubov, *Phys. Rev. B* **2007**, 76, 054522.
- [173] J. Rowell, W. McMillan, *Phys. Rev. Lett.* **1966**, 16, 453.
- [174] J. Rowell, *Phys. Rev. Lett.* **1973**, 30, 167.
- [175] L. Alff, H. Takashima, S. Kashiwaya, N. Terada, H. Ihara, Y. Tanaka, M. Koyanagi, K. Kajimura, *Phys. Rev. B* **1997**, 55, R14757.
- [176] M. Covington, M. Aprili, E. Paraoanu, L. Greene, F. Xu, J. Zhu, C. A. Mirkin, *Phys. Rev. Lett.* **1997**, 79, 277.
- [177] J. Wei, N. C. Yeh, D. Garrigus, M. Strasik, *Phys. Rev. Lett.* **1998**, 81, 2542.
- [178] J. Linder, Y. Tanaka, T. Yokoyama, A. Sudbo, N. Nagaosa, *Phys. Rev. Lett.* **2010**, 104, 067001.
- [179] J. Linder, A. M. Black-Schaffer, A. Sudbo, *Phys. Rev. B* **2010**, 82, 041409.
- [180] A. Black-Schaffer, A. Balatsky, *Phys. Rev. B* **2012**, 86, 144506.
- [181] A. Black-Schaffer, A. Balatsky, *Phys. Rev. B* **2013**, 87, 220506(R).
- [182] F. Parhizgar, A. M. Black-Schaffer, *Phys. Rev. B* **2014**, 90, 184517.
- [183] D. Kuzmanovski, A. M. Black-Schaffer, *Phys. Rev. B* **2017**, 96, 174509.
- [184] M. Rahimi, A. Moghaddam, C. Dykstra, M. Governale, U. Zülicke, *Phys. Rev. B* **2017**, 95, 104515.
- [185] M. R. Aliabad, M. H. Zare, *Phys. Rev. B* **2018**, 97, 224503.
- [186] J. Linder, A. Sudbo, T. Yokoyama, R. Grein, M. Eschrig, *Phys. Rev. B* **2010**, 81, 214504.
- [187] L. P. Gor'kov, E. I. Rashba, *Phys. Rev. Lett.* **2001**, 87, 037004.
- [188] J. Linder, T. Yokoyama, A. Sudbø, M. Eschrig, *Phys. Rev. Lett.* **2009**, 102, 107008.
- [189] J. Linder, A. Sudbø, T. Yokoyama, R. Grein, M. Eschrig, *Phys. Rev. B* **2010**, 81, 214504.
- [190] F. D. M. Haldane, *Phys. Rev. Lett.* **1988**, 61, 2015.
- [191] C. L. Kane, E. J. Mele, *Phys. Rev. Lett.* **2005**, 95, 226801.
- [192] A. M. Black-Schaffer, A. V. Balatsky, *Phys. Rev. B* **2013**, 88, 104514.
- [193] Y. Asano, A. Sasaki, *Phys. Rev. B* **2015**, 92, 224508.
- [194] L. Komendová, A. V. Balatsky, A. M. Black-Schaffer, *Phys. Rev. B* **2015**, 92, 094517.
- [195] L. Komendová, A. M. Black-Schaffer, *Phys. Rev. Lett.* **2017**, 119, 087001.
- [196] Y. Asano, A. A. Golubov, *Phys. Rev. B* **2018**, 97, 214508.
- [197] C. Triola, A. M. Black-Schaffer, *Phys. Rev. B* **2018**, 97, 064505.
- [198] F. Parhizgar, A. M. Black-Schaffer, *Phys. Rev. B* **2014**, 90, 184517.
- [199] B. Sothmann, S. Weiss, M. Governale, J. König, *Phys. Rev. B* **2014**, 90, 220501.
- [200] P. Burset, B. Lu, H. Ebisu, Y. Asano, Y. Tanaka, *Phys. Rev. B* **2016**, 93, 201402.
- [201] H. Ebisu, B. Lu, J. Klinovaja, Y. Tanaka, *Prog. Theor. Exp. Phys.* **2016**, 2016, 083101.
- [202] C. Triola, A. M. Black-Schaffer, *Phys. Rev. B* **2019**, 100, 024512.
- [203] M. M. Ugeda, A. J. Bradley, Y. Zhang, S. Onishi, Y. Chen, W. Ruan, C. Ojeda-Aristizabal, H. Ryu, M. T. Edmonds, H.-Z. Tsai, *Nat. Phys.* **2015**, 12, 92.
- [204] X. Xi, Z. Wang, W. Zhao, J. H. Park, K. T. Law, H. Berger, L. Forr, J. Shan, K. F. Mak, *Nat. Phys.* **2015**, 12, 139.
- [205] Y. S. Gani, H. Steinberg, E. Rossi, *Phys. Rev. B* **2019**, 99, 235404.
- [206] T. Dvir, M. Aprili, C. H. L. Quay, H. Steinberg, *Nano Lett.* **2018**, 18, 7845.